Cell Biol Toxicol (2022) 38:889–911
https://doi.org/10.1007/s10565-021-09617-w

ORIGINAL ARTICLE

The parkinsonian *LRRK2* R1441G mutation shows macroautophagy-mitophagy dysregulation concomitant with endoplasmic reticulum stress

Sokhna M. S. Yakhine-Diop · Mario Rodríguez-Arribas · Saray Canales-Cortés · Guadalupe Martínez-Chacón · Elisabet Uribe-Carretero · Mercedes Blanco-Benítez · Gema Duque-González · Marta Paredes-Barquero · Eva Alegre-Cortés · Vicente Climent · Ana Aiastui · Adolfo López de Munain · José M. Bravo-San Pedro · Mireia Niso-Santano · José M. Fuentes · Rosa A. González-Polo

Received: 30 July 2020 / Accepted: 12 May 2021 / Published online: 31 May 2021

Abstract Autophagy is a mechanism responsible for the degradation of cellular components to maintain their homeostasis. However, autophagy is commonly altered and compromised in several diseases, including neurodegenerative disorders. Parkinson's disease (PD) can be considered a multifactorial disease because environmental factors, genetic factors, and aging are involved. Several genes are involved in PD pathology, among which the *LRRK2* gene and its mutations, inherited in an autosomal dominant manner, are responsible for most genetic PD cases. The R1441G *LRRK2* mutation is, after G2019S, the most important in PD pathogenesis. Our results demonstrate a relationship between the R1441G *LRRK2* mutation and a mechanistic dysregulation of autophagy that compromises cell viability. This altered autophagy mechanism is associated with organellar stress including mitochondrial (which induces mitophagy) and endoplasmic reticulum (ER) stress, consistent with the

Sokhna M. S. Yakhine-Diop and Mario Rodríguez-Arribas contributed equally

Mireia Niso-Santano, José M. Fuentes, and Rosa A. González-Polo are senior co-authors

S. M. S. Yakhine-Diop · M. Rodríguez-Arribas · S. Canales-Cortés · G. Martínez-Chacón · E. Uribe-Carretero · M. Blanco-Benítez · G. Duque-González · M. Paredes-Barquero · E. Alegre-Cortés · M. Niso-Santano (✉) · J. M. Fuentes (✉) · R. A. González-Polo (✉)
Departamento de Bioquímica Y Biología Molecular Y Genética, Facultad de Enfermería Y Terapia Ocupacional, Universidad de Extremadura, Cáceres, Spain
e-mail: mnisosan@unex.es

J. M. Fuentes
e-mail: jfuentes@unex.es

R. A. González-Polo
e-mail: rosapolo@unex.es

S. M. S. Yakhine-Diop
e-mail: smsyakhinediop@unex.es

M. Rodríguez-Arribas
e-mail: mariora@unex.es

S. Canales-Cortés
e-mail: sacanalesc@unex.es

G. Martínez-Chacón
e-mail: guadalupemc@unex.es

E. Uribe-Carretero
e-mail: euribec@unex.es

M. Blanco-Benítez
e-mail: meblancob@alumnos.unex.es

G. Duque-González
e-mail: gemaduque16@gmail.com

M. Paredes-Barquero
e-mail: martapb@unex.es

fact that patients with this mutation are more vulnerable to toxins related to PD, such as MPP^+.

Keywords Autophagy · MAMs · Mitochondrial dysfunction · Neurodegeneration · Parkinson disease

Introduction

The discovery of the gene that encodes the protein leucine-rich repeat kinase 2 (*LRRK2*) has revealed an important component in the etiology of Parkinson's disease (PD) of genetic origin. There are a large number of mutations in this gene that could influence the pathogenesis of this multifactorial and genetically heterogeneous neurodegenerative movement disorder, but only six of these mutations have been shown to contribute a pathogenic component in this disease (Manzoni 2017). Among these mutations, the R1441G mutation is considered the second most important, following only the G2019S mutation.

The R1441G *LRRK2* mutation is endemically present in the Basque region in Spain, and this allelic variant has been found in 13% of diagnosed cases of PD in this region (Liu et al. 2014). The presence of this mutation is generally associated with a decrease in GTPase activity, which is postulated to be responsible for the pathogenic role of this protein, although there is some controversy regarding the role of this activity (Martin et al. 2014). An association has been found between the presence of the R1441G mutation in induced pluripotent stem cells (iPSC) and a failure in the normal regulation of alpha-synuclein as well as a disruption of signaling by the nuclear factor kappa-light-chain-enhancer of activated B cells (NF-κB) pathway (Lopez de Maturana et al. 2016). Moreover, an early axonopathy is found in neurons of transgenic mice that express this mutation (Tagliaferro et al. 2015). Furthermore, the neuronal shortening found in transgenic mice that present this mutation can be reversed through the overexpression of proteins of the 14–3-3 family (Lavalley et al. 2016).

Different studies have suggested that the progressive deterioration of dopaminergic neurons that occurs in PD is caused by incorrect folding and aggregate formation of alpha-synuclein protein, alteration of the autophagy-lysosome system, mitochondrial dysfunction, and/or ER stress (Michel et al. 2016). In this sense, there has been a major effort to clarify

E. Alegre-Cortés
e-mail: evalegrec@unex.es

S. M. S. Yakhine-Diop · M. Rodríguez-Arribas · G. Martínez-Chacón · E. Uribe-Carretero · A. López de Munain · J. M. Bravo-San Pedro · M. Niso-Santano · J. M. Fuentes · R. A. González-Polo
Centro de Investigación Biomédica en Red de Enfermedades (CIBERNED), Madrid, Spain
e-mail: ADOLFOJOSE.LOPEZDEMUNAINARREGUI@osakidetza.eus

J. M. Bravo-San Pedro
e-mail: josemabr@ucm.es

S. M. S. Yakhine-Diop · M. Rodríguez-Arribas · G. Martínez-Chacón · E. Uribe-Carretero · M. Niso-Santano · J. M. Fuentes · R. A. González-Polo
Instituto de Investigación Biosanitaria de Extremadura (INUBE), Cáceres, Spain

V. Climent
Departamento de Anatomía Y Embriología Humana, Facultad de Medicina, Universidad de Extremadura, Badajoz, Spain
e-mail: vcliment@unex.es

A. Aiastui
Cell Culture Platform, Donostia University Hospital, San Sebastián, Spain
e-mail: ana.aiastuipujana@osakidetza.eus

A. Aiastui
Neuroscience Area of Biodonostia Health Research Institute, Donostia University Hospital, San Sebastián, Spain

A. López de Munain
Department of Neurology, Donostia University Hospital, San Sebastian, Spain

A. López de Munain
Ilundain Foundation, San Sebastian, Spain

A. López de Munain
Department of Neurosciences, University of the Basque Country UPV-EHU, San Sebastián, Spain

J. M. Bravo-San Pedro
Departamento de Fisiología, Facultad de Medicina, Universidad Complutense de Madrid, Madrid, Spain

whether dysregulation of the autophagy mechanism in PD is, at least in part, mediated by mutations of the LRRK2 protein. Currently, it is obvious that the relationship exists, but the heterogeneity in the results makes it difficult to obtain a consensus that clarifies the role of this protein in the autophagy mechanism or cellular physiology (Manzoni 2017).

On the one hand, a protective role for autophagy has been described in situations in which it could mitigate the damage caused as a consequence of the accumulation of alpha-synuclein in Lewy bodies (Martinez et al. 2018). On the other hand, it could precede an apoptotic process by increasing susceptibility to death stimuli (Bravo-San Pedro et al. 2013; Yakhine-Diop et al. 2014). The LRRK2 protein has been related to this autophagy mechanism, and its interaction with different proteins has been suggested, such as those of the MEK/ERK pathway (Bravo-San Pedro et al. 2013), the nicotinic acid adenine dinucleotide phosphate (NAADP) pathway (Gomez-Suaga et al. 2012), or BCL-2 (Su et al. 2015). In addition to these studies, many have sought to elucidate the role of certain mutations fundamentally related to kinase activity (G2019S) or GTPase activity (R1441C) in the regulation of autophagy, as well as suppression of LRRK2 kinase activity through the use of specific inhibitors (Bravo-San Pedro et al. 2013; Manzoni et al. 2013a, b; Saez-Atienzar et al. 2014). Furthermore, LRRK2 phosphorylates ras-associated protein 7 (RAB7) (Gomez-Suaga et al. 2014), which is involved in vesicular trafficking from the autophagosome to the lysosome. Additionally, it has been described that the G2019S mutation of this protein blocks the mechanism of chaperone-mediated autophagy both for its own degradation and for that of other substrates degraded by this pathway (Orenstein et al. 2013).

The LRRK2 G2019S mutation has also been linked to mitophagy (selective degradation of mitochondria), as the exacerbation of kinase activity by this mutation entails mitochondrial depolarization. A study by Zhu et al. points out that overexpression of the mutant form induces unc-51 like autophagy activating kinase 1 (ULK1) and dynamin-like protein 1 (DLP1)-dependent mitophagy (Zhu et al. 2013). A connection has also been found between LRRK2 and mitochondrial Rho GTPase 1 (Miro1), a membrane protein that anchors mitochondria to microtubules. LRRK2 forms a complex with this protein, favoring its elimination. However, the G2019S mutant form prevents this removal of Miro1, thus delaying the initiation of mitophagy (Hsieh et al. 2016). In this sense, Cherra et al. have described in mouse cortical neurons expressing either LRRK2 G2019S or R1441C mutations autophagic degradation of mitochondria and dendrite shortening (Cherra et al. 2013). Recently, another study demonstrated that fibroblasts from PD patients with the G2019S LRRK2 mutation exhibit increased mitophagy due to the activation of class III histone deacetylase (HDAC) activities (Yakhine-Diop et al. 2019).

Thus, there is a clear association between LRRK2 and mitochondrial elimination, but it is not yet established whether the regulation is positive or negative, or what the specific roles are of certain mutations, especially G2019S (Schwab et al. 2017).

ER stress has been recognized in different PD cell models (Ganguly et al. 2018). Although the impact of the ER-specific unfolded protein response (UPR) on the degeneration cascade in this disease is just starting to be uncovered, inhibition of protein kinase-like ER kinase (PERK)-mediated ER stress has been shown to protect against PD (Mercado et al. 2018). Moreover, increasing studies are showing the importance of signaling between the mitochondria and ER in PD (Gomez-Suaga et al. 2018). In this sense, several studies point to the structures of membrane exchange between the ER and mitochondria, called mitochondria-associated ER membranes (MAMs), in maintaining calcium signaling and mitochondrial biogenesis. Alterations in MAMs are associated with many diseases, including PD (Rodriguez-Arribas et al. 2017b). Several proteins related to PD are located in MAMs and participate in the regulation of signaling between the mitochondria and ER (Gomez-Suaga et al. 2018). In a PD model of brain astrocytes treated with alpha-synuclein, the LRRK2 G2019S mutants show a sarco/ER Ca^{2+}-ATPase (SERCA) protein alteration that is responsible for ER stress and results in mitochondrial malfunction (Lee et al. 2019). Moreover, it has been described that LRRK2 G2019S regulates the ER-mitochondrial connection through the PERK-mediated ubiquitination pathway (Toyofuku et al. 2020).

There have been no studies on the effect of the R1441G mutation on the macroautophagy/mitophagy/ER stress mechanism. A reduction in its chaperone-mediated autophagy activity has been described in a cell model because

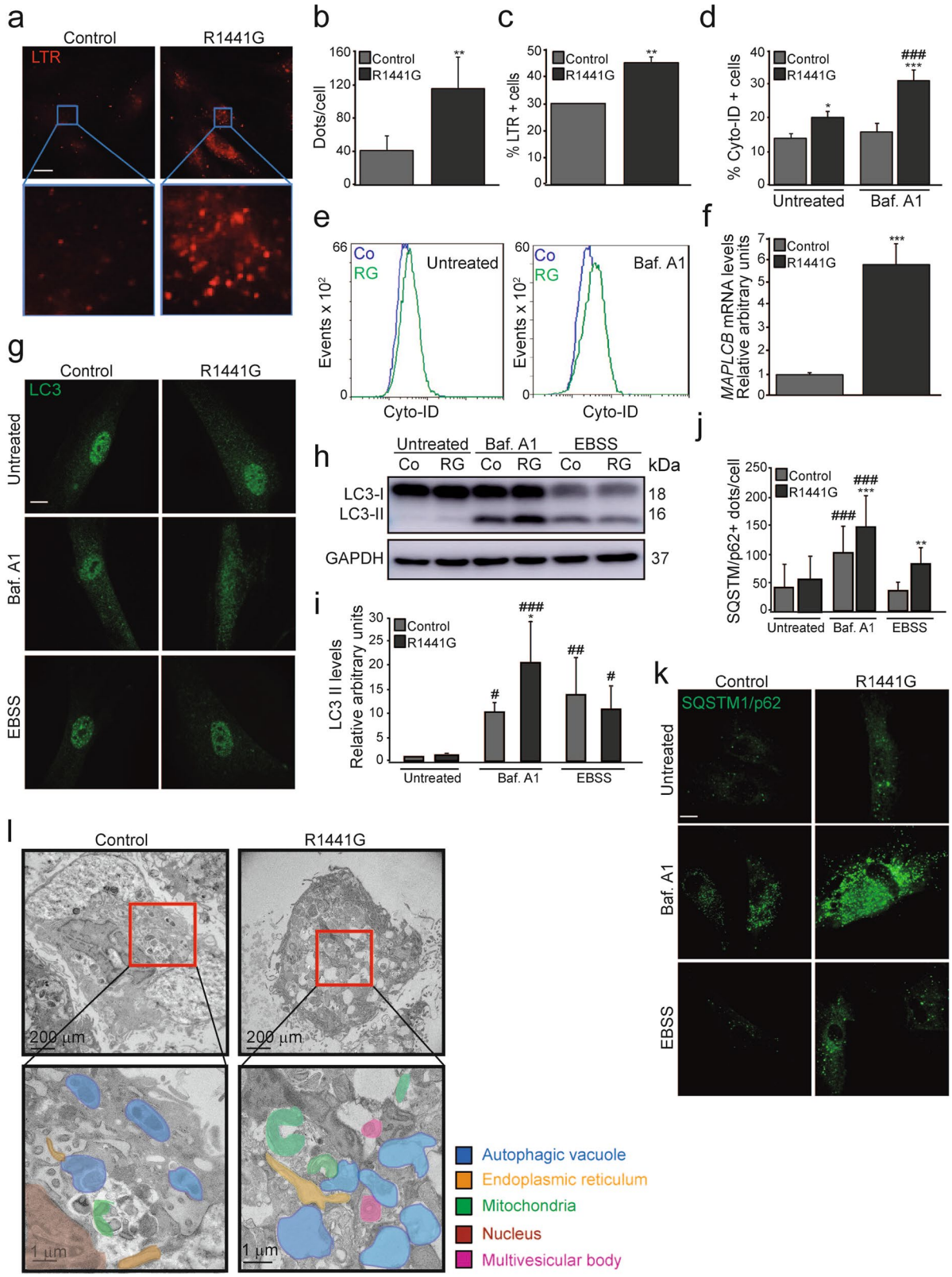
a
Control
R1441G
LTR
b
Dots/cell
Control
R1441G
c
% LTR + cells
d
% Cyto-ID + cells
Untreated
Baf. A1
e
Co
RG
Untreated
Baf. A1
Events x 10²
Cyto-ID
f
MAPLCB mRNA levels
Relative arbitrary units
g
LC3
Untreated
Baf. A1
EBSS
h
Untreated
Baf. A1
EBSS
Co
RG
kDa
LC3-I
LC3-II
GAPDH
18
16
37
i
LC3 II levels
Relative arbitrary units
j
SQSTM/p62+ dots/cell
k
SQSTM1/p62
l
200 µm
1 µm
Autophagic vacuole
Endoplasmic reticulum
Mitochondria
Nucleus
Multivesicular body

◂ **Fig. 1** Determination of lysosomal status and characterization of macroautophagy in human fibroblasts. **a–c** Quantification of the lysosomal mass. **a**, **b** A change of medium was made to the control and R1441G human fibroblasts. At four hours, in vivo staining was performed with lysotracker red (LTR), and the samples were processed to acquire immunofluorescence images, as described in "Materials and methods." Panel **a** shows representative images for each cell line studied. The scale bar represents a length of 10 µm. Panel **b** shows the mean quantification of the number of dots per cell in three independent experiments. At least 200 cells were analyzed per condition. * Indicates statistically significant differences between cell lines (**, $p < 0.01$). **c** DMEM was changed on control and R1441G fibroblasts followed by incubation for 4 h. Next, the cells were detached and stained with the LTR probe as described in "Materials and methods." Next, the cells were analyzed with a FC-500 cytometer (Beckman Coulter), with 10,000 cells processed per condition and three independent experiments performed in triplicate. Panel **c** represents the percentage of cells considered positive for LTR labeling in each cell group studied. * Indicates statistically significant differences between cell lines (**, $p < 0.01$). **d–e** Quantification of the Cyto-ID probe by flow cytometry. Control (Co) and R1441G human fibroblasts (RG) were prestained with Cyto-ID® according to the manufacturer's recommendations and treated or not with Baf. A1 (100 nM) for 4 h. The intensity of the labeling was determined with a FC-500 cytometer (Beckman Coulter), with 10,000 cells analyzed for each condition and independent triplicates performed for each experiment. **d** The graph represents the average percentages of three independent experiments with their standard deviation. The asterisks show significant differences between cell types, while the pound signs reflect differences related to the treatment (*, $p < 0.05$; ***, $p < 0.001$; ###, $p < 0.001$). Panel **e** shows the cytograms of a representative experiment for cells treated or not with Baf. A1. **f** Characterization of LC3 gene expression. RNA was extracted from the control and R1441G fibroblasts, and quantitative PCR was performed in real time for the LC3 gene (*MAPLC3B*). The histogram shows the mean of the expression levels with respect to their loading controls of three independent experiments with their standard deviation. * Represents significant differences between cell lines (***, $p < 0.001$). **g** Determination of LC3 by immunofluorescence. Control and R1441G human fibroblasts were treated or not with Baf. A1 (100 nM) or EBSS for 4 h. Next, the cells were fixed and labeled against the LC3 protein as described in "Materials and methods." Panel g shows representative images of each cell line of three independent experiments for the conditions studied. The scale bar represents a length of 10 µm. **h**, **i** LC3 determination by western blot. Cell lysates from control (Co) and R1441G fibroblasts (RG) treated or not with Baf. A1 (100 nM) or EBSS for 4 h were obtained, and equal amounts of proteins were loaded in 12% polyacrylamide gels as described in "Materials and methods." Panel **h** shows a blot representative of three independent experiments, and panel **i** shows the densitometry histogram. GAPDH was used as a loading control. The asterisks show significant differences between cell types, while the pound signs reflect differences related to the treatment (* or # $p < 0.05$; ##, $p < 0.01$; ###, $p < 0.001$). **j**, **k** Determination of p62 by immunofluorescence. Control and R1441G human fibroblasts were treated or not with Baf. A1 (100 nM) or EBSS for 4 h. Next, the cells were fixed and labeled against the p62 protein as described in "Materials and methods." Panel **l** shows representative images of each cell line of three independent experiments for the conditions studied. The scale bar represents a length of 10 µm. Panel **k** shows the quantification of SQSTM1/p62 protein determined as dots per cell. The asterisks show significant differences between cell types, while the pound signs reflect differences related to the treatment (**, $p < 0.01$; ***, $p < 0.001$; ###, $p < 0.001$). **l** Electron microscopy (EM) images of control and R1441G fibroblasts. The cells were left untreated or treated with Baf. A1 (100 nM) and EBSS for 6 h. The cell pellet was then fixed and processed for EM as described in "Materials and methods." The red boxes show image enlargements

of a possible accumulation of alpha-synuclein aggregates (Orenstein et al. 2013). Although the relationship between GTPase and kinase activity is a controversial issue due to the disparity of published results (Greggio et al. 2009), mutations in the GTPase domain, such as the R1441G mutation, could alter normal autophagic homeostasis and contribute to the pathology and symptomatology of PD.

Our results demonstrate that cells with the *LRRK2* R1441G mutation exhibit an increase in lysosomal markers that is associated with an induction of macroautophagy/mitophagy mechanisms concomitant with increased organellar stress including the mitochondria and ER. These events are responsible for a greater vulnerability to toxins related to PD in the cells of patients with the *LRRK2* R1441G mutation.

Results

Our data revealed that fibroblasts from PD patients who are carriers of the *LRRK2* R1441G mutation (RG) demonstrate important changes in the morphologies of the following organelles and their associated activities: (1) lysosomes, accompanied by an increase in autophagy (Fig. 1); (2) mitochondria, with increasing mitochondrial stress triggering a PINK1-dependent mitophagy response (Figs. 2 and 3); and (3) ER, with induction of an important calcium-dependent ER stress (Figs. 4 and 5). All of these events trigger a consequentially heightened sensibility to the neurotoxin 1-methyl-4-phenylpiridinium (MPP^+) (Fig. 6).

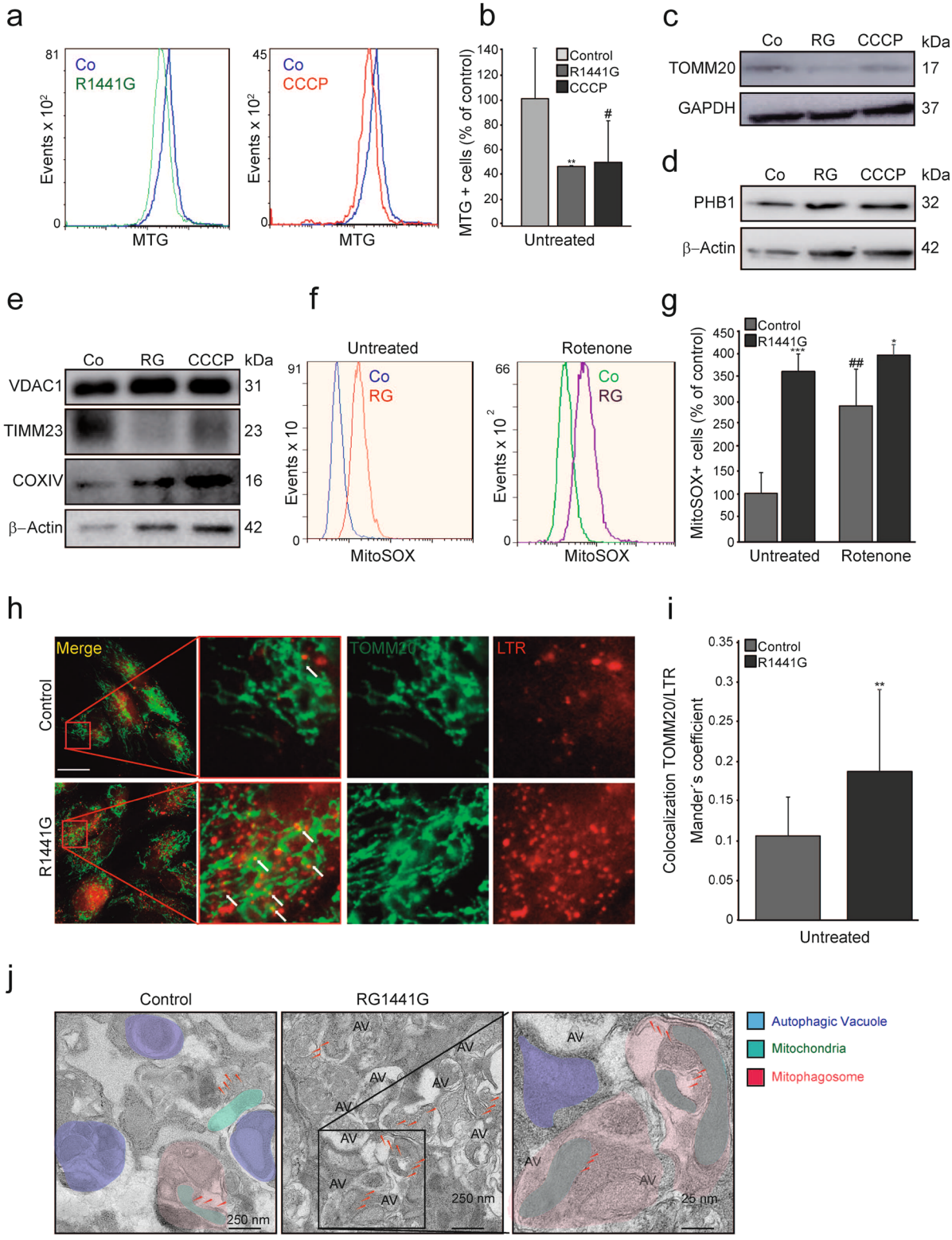
a
Co
R1441G
Events x 10²
MTG
Co
CCCP
b
Control
R1441G
CCCP
MTG + cells (% of control)
Untreated
c
Co RG CCCP kDa
TOMM20
GAPDH
d
PHB1
β–Actin
e
VDAC1
TIMM23
COXIV
f
Untreated
Rotenone
MitoSOX
g
MitoSOX+ cells (% of control)
Untreated
Rotenone
h
Merge
TOMM20
LTR
Control
R1441G
i
Colocalization TOMM20/LTR
Mander´s coefficient
j
Control
RG1441G
AV
250 nm
25 nm
Autophagic Vacuole
Mitochondria
Mitophagosome

◀ **Fig. 2** Determination of mitophagy associated with mitochondrial stress in fibroblasts from PD patients. **a**, **b** Study of mitophagy by flow cytometry. The control (Co) and R1441G fibroblasts (RG) were treated or not with CCCP (10 μM for 4 h), stained with the MTG probe, and analyzed using a FC-500 cytometer, as described in "Materials and methods." A total of 10,000 cells were processed per condition, and three independent experiments were each performed in triplicate. Panel **a** represents the MTG deviation apparent in the RG cells (green) and with the CCCP (red) treatment with respect to the Co cells. Panel **b** represents the percentage of cells considered positive for MTG labeling for each group and condition studied. "*" Indicates significant differences between cell lines, while "#" shows differences between treatments (**, $p < 0.01$; #, $p < 0.05$). **c**–**e** Analyses of specific proteins involved in mitophagy by western blot. The control (Co) and R1441G fibroblasts (RG) were treated or not for 4 h with CCCP. Cell lysates were obtained, and equal amounts of proteins were loaded in 12% polyacrylamide gels as described in "Materials and methods." Panels **c** and **d** show a representative blot of three independent experiments against TOMM20 and PHB1, respectively. β-Actin was used as the loading control. Panel **e** shows a representative blot of three independent experiments with antibodies against VDAC1, TIMM23, and COXIV proteins. β-Actin was used as the loading control. **f**, **g** Analysis of mitochondrial reactive oxygen species (ROS) through MitoSOX labeling. The control and R1441G fibroblasts were treated or not with rotenone (1 μM) for 4 h. Next, the cells were labeled with the MitoSOX probe and processed for flow cytometry according to "Materials and methods." A total of 10,000 cells were processed per condition, and three independent experiments were each performed in triplicate. Panel **f** represents the MitoSOX deviation apparent in the RG cells (red or purple) with respect to the control cells (blue or green) treated or not with rotenone. In panel **g**, the histogram represents the percentage of cells considered positive for MitoSOX labeling (% as control) for each group and condition studied. * Represents differences between cell groups studied, and # shows differences between treatments within the same line (*, $p < 0.05$; ***, $p < 0.001$; ##, $p < 0.01$). **h**–**j** Analysis of mitophagosome and mitolysosome formation. **h**–**i** Study of mitochondria and lysosome colocalization by fluorescence microscopy. The control and R1441G fibroblasts were stained in vivo using the LTR labeling probe. Subsequently, the cells were fixed and labeled against the mitochondrial protein TOMM20 as described in "Materials and methods." Panel **h** shows representative images of each of the cell groups under the conditions studied. The scale bar represents a length of 10 μm. The graphs in panel **i** represent the average of the Mander's coefficient for the proportion of LTR on the TOMM20 label plus the standard deviation. The asterisks show significant differences between cell groups studied (**, $p < 0.01$). **j** Electron microscopy (EM) analysis of vacuolar content. The control and R1441G fibroblasts were treated with Baf. A1 (100 nM) and EBSS for 6 h. Next, the cell pellet was fixed and processed for EM as described in "Materials and methods." The arrows indicate recognizable mitochondria

Fibroblasts from PD patients with *LRRK2* R1441G mutation present an increase in lysosomal and autophagic markers

The lysosomal status was analyzed in our model, showing that the RG group has an increased number of acidic compartments (Fig. 1a–c). Using immunofluorescence (Fig. S2a) as well as western blot (Fig. S2b–g) and mRNA analysis (data not shown), we observed an increase in structural lysosomal proteins LAMP1 (Fig. S2b–c) or LAMP2 (Fig. S2a–c) and lysosomal proteolytic enzymes CTSB (Fig. S2d, f) and CTSD (Fig. S2e, g). These results demonstrate that fibroblasts with the mutation R1441G have an increase in lysosomal markers. For this reason, we performed an in-depth study of autophagy levels in RG cells, observing an activation of macroautophagy exceeding that of control cells. The presence of a higher number of autophagic vacuoles was detected by flow cytometry using the Cyto-ID probe (Fig. 1d, e) or by electron microscopy (EM) analysis (Fig. 1l), correlating a slight increase in the lipidation of LC3, as observed by higher expression levels of the LC3 gene (Fig. 1f), immunofluorescence (Fig. 1g), or western blot (Fig. 1h, i). However, we also observed an accumulation of SQSTM1/p62 protein at basal levels as well as with bafilomycin A1 treatment (Baf. A1), observed as dots per cell, in the RG group (Fig. 1j, k). Baf. A1 is a V-ATPase inhibitor that causes an increase in lysosomal/vacuolar pH and ultimately blocks the fusion of autophagosomes with the lysosomes. In addition, the detection of p-mTOR and its substrate p-S6 show that the autophagy observed in the RG group is mTOR independent. This level of phosphorylation is accompanied by a slight increase of autophagy-related proteins (ATG5 or BECN1) in the RG group (Fig. S2h–m). In this sense, both pharmacological (using the 3MA inhibitor) and genetic (with the use of specific siRNAs) inhibitions corroborated the essential role of these proteins in RG group mediated-autophagy (data not shown). It is important to note that RG fibroblasts respond to both autophagy induction (deprivation with Earle's Balanced Salt Solution [EBSS] medium) and inhibition (Baf. A1) (Figs. 1g–k and S2), indicating that autophagy flux is not blocked at this level.

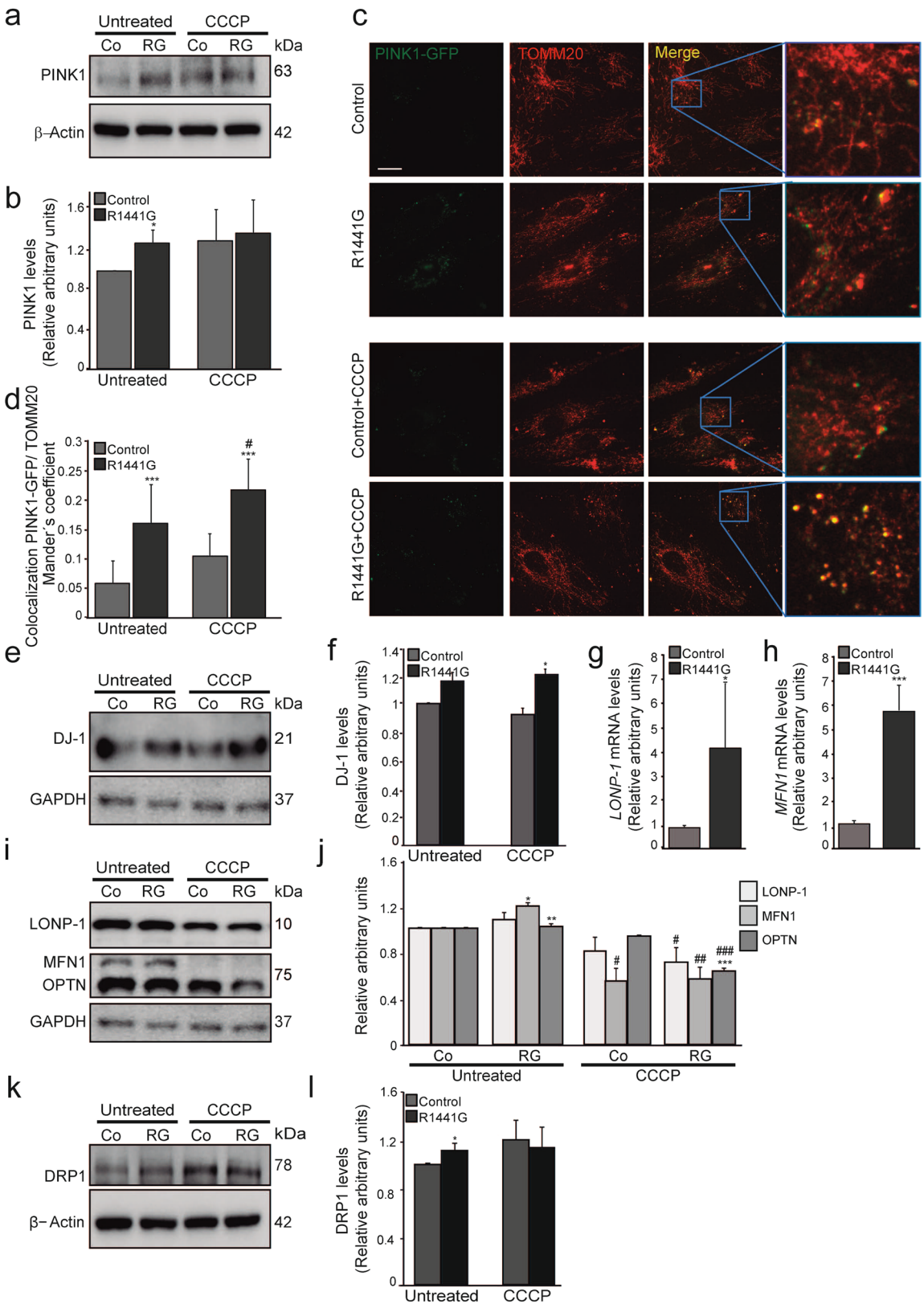
a
Untreated
CCCP
Co
RG
Co
RG
kDa
PINK1
63
β-Actin
42
b
Control
R1441G
PINK1 levels
(Relative arbitrary units)
Untreated
CCCP
c
PINK1-GFP
TOMM20
Merge
Control
R1441G
Control+CCCP
R1441G+CCCP
d
Colocalization PINK1-GFP/ TOMM20
Mander's coefficient
Control
R1441G
Untreated
CCCP
e
DJ-1
21
GAPDH
37
f
DJ-1 levels
(Relative arbitrary units)
g
LONP-1 mRNA levels
(Relative arbitrary units)
h
MFN1 mRNA levels
(Relative arbitrary units)
i
LONP-1
10
MFN1
OPTN
75
GAPDH
37
j
Relative arbitrary units
LONP-1
MFN1
OPTN
k
DRP1
78
β- Actin
42
l
DRP1 levels
(Relative arbitrary units)

◂ **Fig. 3** Study of proteins involved in the induced mitophagy of R1441G fibroblasts. **a**, **b** Analysis of the PINK1 protein by western blot. Cell lysates from control (Co) and R1441G fibroblasts (RG) treated or not with CCCP (10 μM for 4 h) were obtained, and equal amounts of proteins were loaded in 12% polyacrylamide gels as described in "Materials and methods." The panels show representative western blot (**a**) and the densitometry histograms performed (**b**) of PINK1 protein of three independent experiments. * Show significant differences between cell groups studied (*, $p < 0.05$). β-Actin was used as a loading control. **c**, **d** Colocalization between PINK1 and TOMM20. Control and R1441G fibroblasts were modified to overexpress PINK1-GFP, as described in "Materials and methods." Twenty-four hours post transfection, the cells were treated or not with CCCP (10 μM for 4 h). Panel **c** shows representative images for each of the studied conditions. The scale bar represents 10 μm. Panel **d** show the staining of PINK1-GFP that overlaps with the TOMM20 labeling expressed by the Mander's coefficient. * Represents significant differences between the cell lines studied, and # shows differences between treatments within the same line (***, $p < 0.001$; #< 0.05). **e**, **f** Analysis of the DJ-1 protein by western blot. The control (Co) and R1441G fibroblasts (RG) were treated or not for 4 h with CCCP. Panel **e** shows the representative blot of three independent experiments against DJ-1. GAPDH was used as the loading control. Panel **f** shows densitometry of the representative western blot shown in panel **e**. * Show significant differences between cell groups studied (*, $p < 0.05$). **g**, **h** Characterization of mitochondrial genes. An extraction of control and R1441G fibroblast genomic RNA was performed, and quantitative PCR was performed in real time for the *LONP1* (**g**) and *MFN1* (**h**) genes as described in "Materials and methods." *GAPDH* was used as an endogenous control for gene expression. The histograms show the means of the expression levels with respect to their loading controls of three independent experiments, with standard deviation. * Represents significant differences between cell lines studied for the same gene (*, $p < 0.05$; ***, $p < 0.001$). **i**–**l** Characterization of mitochondrial proteins by western blot. The control (Co) and R1441G fibroblasts (RG) were treated or not for 4 h with CCCP. Cell lysates were obtained, and equal amounts of proteins were loaded in 12% polyacrylamide gels as described in "Materials and methods." Panels **i** and **k** show blots representative of three independent experiments. GAPDH or β-Actin was used as a loading control. Panels **j** and **l** show densitometric analysis of the representative western blot shown in panels **i** and **k** respectively. * Show significant differences between cell groups studied (*, $p < 0.05$; **, $p < 0.01$; ***, $p < 0.001$), and # shows differences between treatments within the same line (#, $p < 0.05$; ##, $p < 0.01$; ###, $p < 0.001$)

LRRK2 R1441G fibroblasts show an increase in mitochondrial stress and mitophagy-specific activity

We focused on the possibility of mitochondrial damage resulting in selective degradation through mitophagy. We started by analyzing the mitochondrial status in RG fibroblasts using the MTG label (Mauro-Lizcano et al. 2015). Under basal conditions, RG fibroblasts showed a significant 60% mitochondrial mass reduction compared to control cells, that is even higher in the presence of the mitochondrial uncoupler, carbonyl cyanide 3-chlorophenylhydrazone (CCCP; Fig. 2a, b). The western blot analysis of the mitochondrial outer and inner membrane proteins (Figs. 2c–e and S3a–e), as well as representative EM images (Fig. S3f), confirmed the evidence of a lower mitochondrial content in the RG cells. Moreover, we measured the levels of mitochondrial stress present in the RG cells compared to the control cells (Co), and we observed an increase in the percentage of cells with mitochondrial reactive oxygen species (ROS), especially superoxide, by MitoSOX staining (Figs. 2f, g and S3g). Interestingly, this rise in the basal levels of mitochondrial stress is comparable to the increase observed after stimulation with the mitochondrial complex I inhibitor rotenone in control and RG cells, and non-synergistic effects of rotenone were observed in cells from RG patients (Figs. 2f, g and S3g). Given the reduced level of mitochondrial mass, we investigated if mitophagy is activated in these cells as a protective mechanism to remove the damaged mitochondria responsible for the oxidative stress observed. Therefore, to study mitophagy in the fibroblasts from PD patients with the R1441G mutation, we analyzed the presence of the mitophagosomes (autophagic vacuoles [AV] with mitochondrial content) in the EM images. The results indicate that human RG fibroblasts have a greater number of mitochondria within AVs than the control group (Co) (Fig. 2j). Moreover, the results of colocalization of mitochondria and lysosomes using specific labels (translocase of outer mitochondrial membrane 20 [TOMM20] and lysotracker red [LTR], respectively) (Fig. 2h, i) revealed that, in fact, there was a significant increase in the convergence of both, as determined by Mander's coefficient, in RG fibroblasts with respect to the control cells. Treatment with CCCP mitigated these differences between the two groups (Fig. S3h, i). Moreover, the levels of TOMM20 and TIMM23 were increased in response to Baf. A1 treatment in RG group (Fig. S3j, k). All of these results suggest

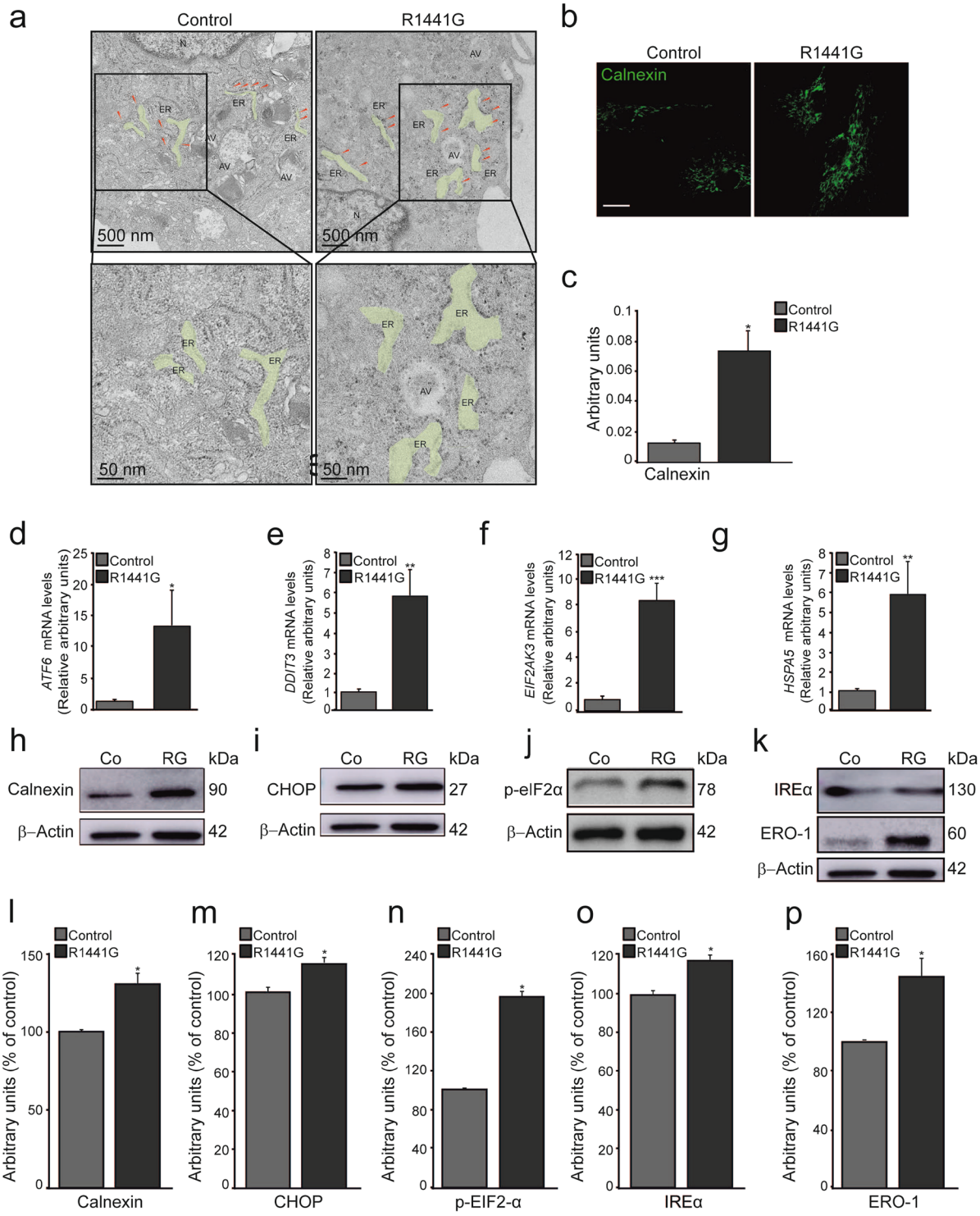

that the mitophagy mechanism could play an important role in RG fibroblasts.

The R1441G fibroblasts undergo PINK1-dependent mitophagy

◂ **Fig. 4** Characterization of ER stress. **a** ER analysis by electron microscopy (EM). The cell pellet from control and R1441G fibroblasts was fixed and processed for EM as described in "Materials and methods." Representative images are shown with magnification for each cell group studied. The arrows and colored structures in the image point to the ER. AV: Autophagic vacuoles; ER: Endoplasmic reticulum; N: Nucleus. **b**, **c** Calnexin determination by immunofluorescence (IF). The control and R1441G fibroblasts were fixed and labeled for detection of the protein calnexin, as described in "Materials and methods." Panel **b** shows representative images for each cell group. The scale bar symbolizes 10 µm. Panel **c** shows the fluorescence analysis of each cellular group represented as arbitrary units. At least 200 cells were analyzed per condition. * Represents significant differences between cell lines (*, $p < 0.05$). **d–g** Characterization of expression levels of genes involved in ER stress. Control and R1441G fibroblast RNA was extracted, and real-time quantitative PCR was performed for the *ATF6* (**d**) *CHOP* (*DDIT3*, **e**), *PERK* (*EIF2AK3*, **f**), and *GRP78* (*HSPA5*, **g**) genes, as described in "Materials and methods." *GAPDH* was used as an endogenous control of gene expression. The histograms show the means of three independent experiments and their standard deviation. * Represents significant differences between cell lines studied for the same gene (*, $p < 0.05$; **, $p < 0.01$; ***, $p < 0.001$). **h–p** Characterization of ER proteins by western blot. Cell lysates from control (Co) and R1441G fibroblasts (RG) were obtained, and equal amounts of proteins were loaded in 12% polyacrylamide gels as described in "Materials and methods." The panels show representative western blots and the densitometry histograms performed of calnexin (**h**, **j**), CHOP (**i**, **m**), p-eIF2α (**k**, **n**), and IREα and ERO-1 (**k**, **o**, **p**) proteins of three independent experiments, respectively. β-Actin was used as a loading control. * Represents significant differences between cell lines (*, $p < 0.05$)

The most studied and implicated mitophagy pathway in PD is the PINK1-parkin pathway (Ivankovic et al. 2016; Koentjoro et al. 2017). Figure 3a, b shows an increase in endogenous PINK1 protein levels in the RG fibroblasts, with respect to the control group, in both untreated and CCCP-treated cells. To analyze the importance of this axis in our model, an overexpression of the chimeric protein PINK1-GFP was performed with the mitochondrial protein TOMM20 to determine the involvement of PINK1 in this process. The results obtained show a significant augmentation in the recruitment of PINK1 to the mitochondrial membrane in the RG fibroblasts, with respect to the control group, in both untreated and CCCP-treated cells (Fig. 3c, d). Next, the DJ-1 protein was studied (Fig. 3e, f). In parallel to the PINK1/parkin pathway, DJ-1 serves to maintain mitochondrial function and autophagy in the presence of an oxidative environment (McCoy and Cookson 2011). Figure 3e shows a slight increase in DJ-1 levels in the RG group when treated or not with CCCP, compared with the control group. Other mitochondrial proteins were also investigated, including lon peptidase 1 (LONP1) (Zurita Rendon and Shoubridge 2018), a mitochondrial matrix protease; mitofusin 1 (MFN1) (Burte et al. 2015), an outer-membrane protein involved in mitochondrial fusion; and optineurin (OPTN), an adaptor that translocates to mitochondria during mitophagy (Weil et al. 2018). The results reveal a decrease in the levels of these proteins in the RG group treated with CCCP (Fig. 3f, j), suggesting that RG group is more sensitive to mitophagy induction (or CCCP treatment). However, although LONP1 and MFN1 protein levels were not remarkably modulated under basal conditions, this could be due to the significant increase in their mRNA levels (Fig. 3g–h). The GTPase dynamin-related protein 1 (DRP1), a protein involved in the process of mitochondrial fission (Fonseca et al. 2019), is upregulated in RG fibroblasts, treated or not with CCCP (Fig. 3k, l). Therefore, these mitochondrial proteins could play an important role in the mitophagy observed in the RG group.

Fibroblasts from PD patients with the R1441G mutation show greater endoplasmic reticulum stress than the control group

There is increasing evidence of the importance of signaling between mitochondrial and ER stress in PD pathology (Gomez-Suaga et al. 2018). We have observed changes at the lysosomal and mitochondrial levels in RG cells; therefore, we wanted to assess the state of the ER in our model. EM analysis of the ER structure was performed, and as observed in Fig. 4a, the RG group showed greater ER swelling compared to the control group. This fact led us to analyze other additional proteins that should be involved in ER stress. An analysis of calnexin (an integral ER membrane protein) was performed as shown in Fig. 4b, c, h, l. These panels show an increase in the levels of this ER protein in the RG group compared to the control group. Moreover, quantitative PCR of some genes involved in ER homeostasis was performed in both cell groups (co and RG) (Fig. 4d–g). These results show an increase in gene expression related to ER stress in the RG group compared to control cells. This increase detected in the RG group agreed with the levels of ER stress-related proteins shown

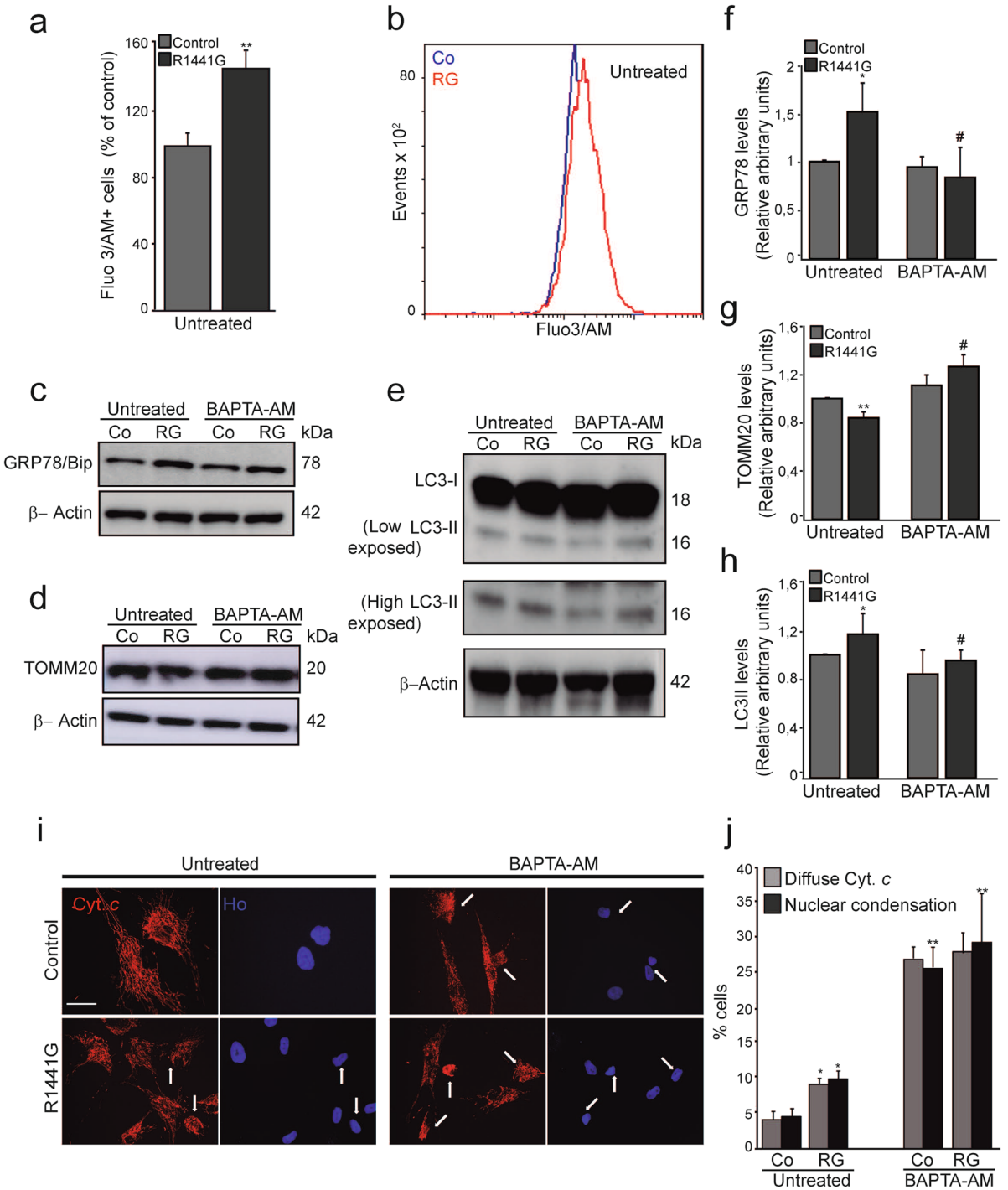

in Fig. 4i–k (and Fig. 4m–p) such as CHOP, IREα, ERO-1, and p-eIF2α.

Cytosolic calcium chelation inhibits the mitophagy observed in cells with the R1441G mutation

There is a significant interconnection between the

◂ **Fig. 5** Calcium release-induced mitophagy in R1441G *LRRK2* fibroblasts. **a**, **b** Determination of cytosolic calcium. The control (Co) and R1441G fibroblasts (RG) were detached and labeled with the Fluo-3 probe as described in "Materials and methods." Cells (10,000 events per condition) were analyzed with the FC-500 cytometer (Beckman Coulter). The percentage of the population positive for Fluo-3 retention is shown in panel **a**, and panel **b** shows the cytograms of a representative experiment. * Represents significant differences between cell lines (**, $p < 0.01$). **c**–**h** Analysis of GRP78/Bip, TOMM20, and LC3 proteins by western blot in the presence or absence of BAPTA-AM. The control group (Co) and R1441G fibroblasts (RG) were treated or not for 4 h with BAPTA-AM (5 μM). Cell lysates were obtained, and equal amounts of proteins were loaded in 12% polyacrylamide gels as described in "Materials and methods." Panels show representative western blots and the densitometry histograms of GRP78/Bip (**c**, **f**), TOMM20 (**d**, **g**), and LC3 (**e**, **h**) proteins of three independent experiments, respectively. β-Actin was used as a loading control. The asterisks show significant differences between cell types, while the pound signs reflect differences related to the treatment (* or #, $p < 0.05$; ** or ##, $p < 0.01$). **i**, **j** Determination of cytochrome *c* alteration and nuclear condensation in the presence of BAPTA-AM. The control (Co) and R1441G fibroblasts (RG) were treated or not with BAPTA-AM for 18 h. Next, the cells were fixed and labeled against cytochrome *c* (Cyt *c*), and the nuclei were stained with Hoechst 33342 (Ho), as described in "Materials and methods." Panel **i** shows representative images of each of the lines and conditions studied. The scale bar represents a length of 10 μm. The arrows indicate positive events. A total of 200 cells were analyzed for each condition. In **j**, the histogram shows the percentage of cells with diffuse Cyt *c* and nuclear condensation. * Shows significant differences between cell groups studied (*, $p < 0.05$; **, $p < 0.01$)

mitochondria, ER, and calcium, linking all of them both biochemically and physically (de Brito and Scorrano 2008; Giacomello et al. 2020). The ER molecular chaperone glucose-regulated protein 78 (GRP78)/Bip is involved in calcium buffering in the ER lumen (Lievremont et al. 1997) and participates in the regulation of ER stress-mediated autophagy (Kania et al. 2015). This protein is modulated by glucose availability and Ca^{2+} concentration (Kitzman et al. 1996). Calcium homeostasis perturbation has been postulated as one of the major factors influencing the altered autophagy observed in certain neurodegenerative processes, such as PD (Bezprozvanny 2009; Mattson 2007). To analyze the cytosolic calcium levels in our model, we used the Fluo3/AM fluorophore, which binds to the calcium present in the intracellular space. Figure 5a, b shows an increase in the percentage of Fluo3/AM positive cells in RG group compared with control. The increased calcium observed in RG cells could be responsible for the increased levels of GRP78/Bip detected in this cell group (Fig. 5c, f) because the protein levels in the presence of a chelator of this cation, BAPTA-AM, were diminished.

In the same way, to analyze the importance of increased cytosolic calcium in the mitophagy-induced RG cells, we treated the cells with BAPTA-AM and studied the LC3 and TOMM20 protein levels. The results show an increase in mitochondrial mass as detected by a higher level of the TOMM20 protein (Fig. 5d, g) and a decrease in the LC3 isoform II (Fig. 5e, h) in the presence of the Ca^{2+} chelator. These findings suggest that GRP78/Bip modulation by cytosolic calcium could play an important role in the mitophagy induced in cells with the R1441G mutation. On the other hand, treatment with BAPTA-AM resulted in an increase in the percentage of cells with mitochondrial instability of the cytochrome c (Cyt *c*) protein and nuclear condensation (Fig. 5i, j).

The mitochondrial stress observed in the R1441G fibroblasts is associated with a higher cellular sensitivity

Finally, consistent with all of the results shown above, RG cells demonstrated an increased sensitivity at basal levels and in the presence of the parkinsonian toxin MPP^+ as determined by immunofluorescence (Fig. 6a, b) and flow cytometry assays (Fig. 6c, d). Increased mitochondrial instability of the Cyt *c* protein and the presence of nuclei with condensed chromatin were observed in the RG fibroblasts (Fig. 6a, b). Moreover, these cells displayed a decreased mitochondrial membrane potential (MMP) (detected by the decreased retention capacity of the $DiOC_6(3)$ in mitochondria) (Fig. 6c) and an increase in cell death (detected by flow cytometry using PI) (Fig. 6d), compared to the fibroblasts from healthy individuals.

Once the greater sensitivity and the presence of a mitochondrial alteration in RG human fibroblasts were confirmed, we deepened the study of the mitochondria using a specific mitochondrial damage inducer, CCCP, to determine if this mitochondrial damage could be a sensor of the induction of a lysosome-specific degradative pathway. Therefore, we monitored the lysosomes with LTR and the MMP with $DiOC_6$ (3) (Fig. 6e, f). The results show that the RG group has a higher percentage of the cell population containing greater

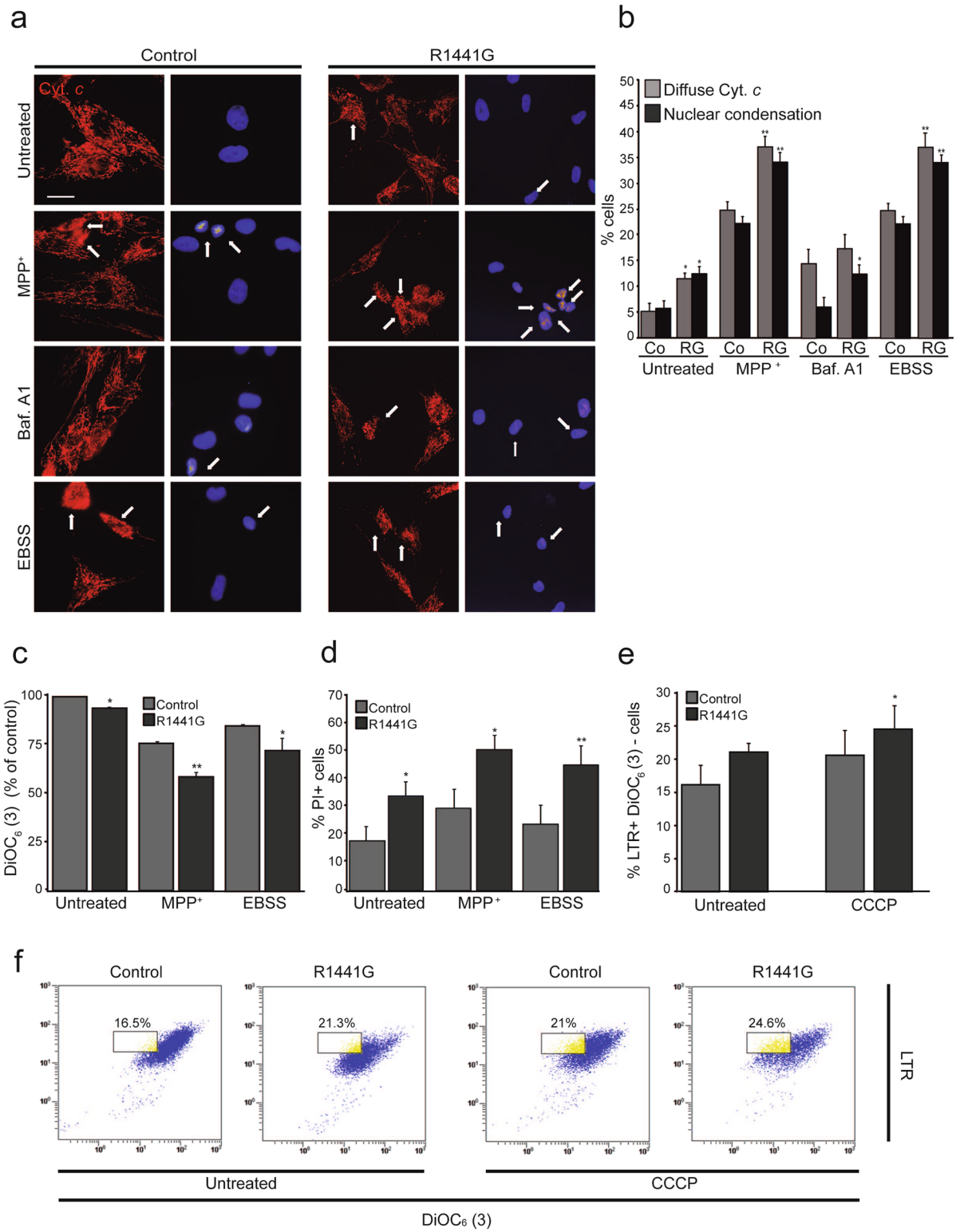
a
Control
R1441G
Cyt. c
Untreated
MPP+
Baf. A1
EBSS
b
Diffuse Cyt. c
Nuclear condensation
% cells
Co RG Co RG Co RG Co RG
Untreated MPP+ Baf. A1 EBSS
c
DiOC6 (3) (% of control)
Control
R1441G
Untreated MPP+ EBSS
d
% PI+ cells
Control
R1441G
Untreated MPP+ EBSS
e
% LTR+ DiOC6 (3) - cells
Control
R1441G
Untreated CCCP
f
Control
R1441G
Control
R1441G
16.5%
21.3%
21%
24.6%
LTR
Untreated
CCCP
DiOC6 (3)

◂ **Fig. 6** Determination of cellular sensitivity in the presence of MPP^+ and autophagic modulators. **a**, **b** Determination of Cyt *c* alteration and nuclear condensation. The control (Co) and R1441G fibroblasts (RG) were treated or not with MPP^+, Baf. A1, or EBSS for 18 h. Next, the cells were fixed and labeled against Cyt *c*, and the nuclei were stained with Hoechst 33342 (Ho), as described in "Materials and methods." Panel **a** shows representative images of each of the lines and conditions studied. The scale bar represents a length of 10 µm. The arrows indicate positive events. A total of 200 cells were analyzed for each condition. In **b**, the histogram shows the percentage of cells with diffuse Cyt *c* and nuclear condensation. * Shows significant differences between cell groups studied (*, $p < 0.05$; **, $p < 0.01$). **c**, **d** Determination of cell viability by flow cytometry. The control group and R1441G fibroblasts were treated or not with MPP^+ or EBSS for 18 h. Next, the cells were detached and labeled with the $DiOC_6(3)$ probe and propidium iodide (PI), as described in "Materials and methods." Cells (10,000 events per condition) were analyzed with the Beckman Coulter FC-500 cytometer. The percentage of the population positive for $DiOC_6(3)$ and PI retention is shown in panels **c** and **d**, respectively. * Shows significant differences between cell groups studied (*, $p < 0.05$; **, $p < 0.01$). **e**, **f** Study of the correlation between the loss of mitochondrial membrane potential and lysosomes. The control group and R1441G fibroblasts were treated or not with CCCP (10 µM) for 4 h. Next, the cells were detached and stained with the $DiOC_6(3)$ and LTR probes as described in "Materials and methods." Cells (10,000 events per condition) were analyzed with the Beckman Coulter FC-500 cytometer. In **e**, the histogram shows the percentage of the cell subpopulation with low retention of the $DiOC_6(3)$ probe and high retention of LTR over the total events of three independent experiments. * Shows significant differences between cell groups studied (*, $p < 0.05$). Panel **f** shows a graph of the cell population for each pool and the condition studied in a representative experiment

lysosomal mass (LTR^+ cells) and lower MMP ($DiOC_6(3)^-$ cells) than the Co group, in the presence of CCCP. Moreover, the sensitivity of RG fibroblasts was more evident in the presence of both an inducer (deprivation with EBSS medium) and an inhibitor (Baf. A1) of autophagy. This sensitivity was determined by observing the instability of mitochondrial Cyt *c* and nuclear condensation (Fig. 6a, b). Furthermore, the deprivation of nutrients produced a decrease in the retention capacity of $DiOC_6(3)$ staining in the mitochondria in R1441G fibroblasts (Fig. 6c) and an augmentation of PI incorporation (Fig. 6d).

Taken together, these results suggest the possible role of the lysosome and mechanisms associated with this organelle, such as autophagy, as responsible for the differences observed between the cells.

Discussion

The lack of effectiveness in PD treatments described so far suggests that a greater knowledge of the cellular pathways involved in the etiology of PD is necessary to promote alternative and synergistic therapeutic strategies that improve symptoms or delay disease progression. In this sense, the association of PD with dysregulated cellular mechanisms such as macroautophagy or mitophagy in several cellular and animal models, including those of the LRRK2 protein (Cerri and Blandini 2019), raises the possibility of pharmacologically modulating these mechanisms to mitigate clinical symptoms.

Many studies have been conducted on PD pathogenesis in association with the *LRRK2* G2019S mutation and autophagy deregulation (Bravo-San Pedro et al. 2013; Mortiboys et al. 2010; Papkovskaia et al. 2012; Plowey et al. 2008; Su et al. 2015; Su and Qi 2013; Yakhine-Diop et al. 2014, 2019; Zhu et al. 2013). However, little evidence exists on the effects of the *LRRK2* R1441G mutation in PD.

In this article, we have shown that cells from patients with the *LRRK2* R1441G mutation exhibit an increase in lysosomal markers, associated with an induction of macroautophagy (Figs. 1 and S1), stress and mitochondrial damage associated with mitophagy (Figs. 2, S2, and 3), and concomitant with ER stress (Fig. 4). These facts are reversed, in part, by a blockage of the calcium cascade in the cytosol with the chelator BAPTA-AM (Fig. 5). Additionally, we demonstrate that these cells show a greater sensitivity to the exposure of toxins related to PD and that the inhibition of the autophagic processes accentuates this sensitivity (Fig. 6).

To date, the mechanism by which LRRK2 is implicated in the normal physiology of the autophagy mechanism and the precise way in which its activity variation dysregulates this physiology have yet to be determined.

Our results show an increase in both activity and number of lysosomes as well as lysosomal mass in the cells of patients with the *LRRK2* R1441G mutation. This increase is correlated with a high number of LC3-positive autophagic structures, and an increase in the p62 protein, probably due to an increased signaling of the material to be degraded (Sahani et al. 2014). The macroautophagy induction observed is induced in an ATG5-BECN1-dependent manner, with

an increase in p-mTOR. One study with the *LRRK2* R1441G mutation (Manzoni et al. 2013b) indicates a lack of response to p-mTOR modulation in basal conditions and in the absence of nutrients, in which the p62 protein is not modulated. The most likely explanation for these different results is the use of different experimental conditions when establishing nutrient deprivation.

The induction of the autophagy mechanism observed in *LRRK2* R1441G mutants could be interpreted as an organism response to an external situation that alters its cellular homeostasis as a consequence of a pathological accumulation of misfolded proteins (Martinez et al. 2018) or organellar damage (Cuervo et al. 2004; Lynch-Day et al. 2012; Orenstein et al. 2013). In fact, PARK genes are involved in mitophagy regulation (Melser et al. 2015). PINK1, parkin, and LRRK2 pathogenic mutations are determining factors in mitochondria status of PD models (Bonello et al. 2019; Larsen et al. 2018; Schapira 2008).

It has been described that overexpression of both the wild type and the *LRRK2* G2019S mutation causes mitochondrial fragmentation mediated by its interaction with dynamin-like protein-1 (DLP-1) (Niu et al. 2012). In addition, endogenous LRRK2 can interact with regulators of mitochondrial fission and fusion (such as Drp1, OPA1, and MFN) (Su and Qi 2013; Wang et al. 2012). In R1441G LRRK2 fibroblasts, the increasing level of Drp1 and MFN1 could be attributed to the maintenance of mitochondrial dynamic and the balance in mitochondrial fusion/fission during the basal mitophagy process. The latter is totally disturbed by CCCP treatment as reflected by the decrease of MFN1 (Fig. 3i, j), while DRP1 was increasing (Fig. 3k, l).

However, some studies defend that a blockade of this mechanism mediated by the LRRK2 protein is responsible for cell damage and degeneration. In this regard, one study suggests that the inhibition of autophagy and mitophagy caused by LRRK2 overexpression is responsible for the degeneration of Purkinje cells in diabetic rats (Yang et al. 2014).

Our results exhibit decreases in both mitochondrial mass and inner and outer mitochondrial membrane proteins in the presence of the R1441G mutation. This decrease in mitochondrial markers is correlated with an increase in mitochondrial stress and the existence of mitolysosomes. Moreover, we have also shown that this mitophagy mechanism is PINK1/DJ1 dependent. The PINK1 and DJ-1 proteins are essential for maintaining the homeostasis of mitochondria, which is achieved by regulating mitochondrial fusion and fission. For severely damaged mitochondria that are beyond repair, the PINK1 pathway is used to direct their clearance by mitophagy (Mishra and Chan 2016). DJ-1 has been regarded as a redox sensor, with potential roles in mitochondrial homeostasis (Canet-Aviles et al. 2004). It has been described that in both fibroblasts and neurons, mitochondrial DJ-1 level is elevated following oxidative damage and may act in a pathway parallel to that of the PINK1/parkin pathway (van der Merwe et al. 2015).

Our cell model is in an induced mitophagy scenario, consistent with that described by several studies (Niu et al. 2012; Su and Qi 2013; Zhu et al. 2013), which could identify this as an attempt to regulate mitochondrial homeostasis. If the mitochondria are pathologically altered in our PD model, there may be an attempt by the cell to try to remove these damaged mitochondria to preserve cellular integrity. However, if ineffective, that increase in ROS and mitochondrial damage could contribute to the increase in cellular sensitivity already described. Given that there are no previous reports suggesting possible mitochondrial and mitophagy alterations in Parkinson's patients' cells carrying R1441G, it should be highlighted that there are common characteristics in specific models of mitochondrial involvement in PD that are mediated by the G2019S mutation of *LRRK2* and that develop common symptomatology in PD patients (Somme et al. 2015).

Calcium homeostasis is very important in the connections between the mitochondria and ER. Altered calcium homeostasis has been consistently observed in neurological diseases. In this sense, it has been described that altered ER-mitochondria contact affects mitochondrial calcium homeostasis and contributes to neurodegeneration in several disease models, including in PD (Lee et al. 2018). For example, a study has demonstrated that enhanced parkin levels favor ER-mitochondria crosstalk and guarantee calcium transfer to sustain cell bioenergetics (Cali et al. 2013). Either calcium chelators or inhibitors of voltage-gated L-type calcium channels prevented mitochondrial degradation and dendrite shortening in mouse cortical neurons expressing LRRK2 mutations (Cherra et al. 2013). Moreover,

in a *Drosophila* PD model, it has been described that Ca^{2+} transport from the ER to mitochondria critically regulates mitochondrial Ca^{2+} homeostasis in dopaminergic neurons and that the PD-associated PINK1 protein modulates this process (Lee et al. 2018).

Studies linking LRRK2 protein to ER stress are emerging. In a *Caenorhabditis elegans* model lacking the LRRK2 homolog, it has been suggested that this protein is critical for preventing ER stress and spontaneous neurodegeneration (Samann et al. 2009). It has also been suggested that LRRK2 regulates anterograde ER-Golgi transport by anchoring Sec16A at ER exit sites, leading to a reduction in ER stress (Cho et al. 2014). Another study has described that LRRK2 regulates ER-mitochondrial tethering through the PERK-mediated ubiquitination pathway (Toyofuku et al. 2020).

Moreover, in neuroblastoma cells and *C. elegans* dopaminergic neurons, expression of wild-type LRKK2 protects from hydroxydopamine and/or human alpha-synuclein, respectively, by supporting upregulation of GRP78/Bip (Yuan et al. 2011). Despite these interesting findings, the possible contribution of ER stress to the pathogenic manifestations of mutant LRKK2 in mammalian cells has not yet been addressed. Our results reveal alterations of the ER in patient fibroblasts with the *LRRK2* R1441G mutation and an increase in the expression of ER-stress-related proteins with direct implication with PD. In this sense, a possible failure of protective folding has been found in a PD model induced by rotenone (Lin et al. 2018). There is abundant evidence of a direct relationship between autophagy regulation and the UPR-mediated response (Chung et al. 2016), so that accumulation of misfolded proteins (as occurs in PD) could lead to an increase in this response in the RG group.

Moreover, we have described results that demonstrate a greater amount of cytosolic calcium in the presence of the R1441G mutation. This fact is in parallel with an increase in the GRP78/Bip levels, one of the most important chaperones that regulate ER-stress-mediated autophagy modulated through cytosolic calcium levels (Wong et al. 2013).

The administration of a chelator of this cation, such as BAPTA-AM, reverses, in part, the increase of GRP78/Bip levels and the observed mitophagy, highlighting the importance of calcium in this model. However, this fact causes an increase, both in mitochondrial instability and in nuclear damage, in control and RG fibroblasts. The increase in cellular sensitivity in the presence of BAPTA-AM has already been demonstrated by other authors recently (Williams et al. 2013). They have demonstrated that the presence of the chelator relieved MG132-induced ER stress, but not rescue MG132-induced apoptosis, possibly as a consequence of blocking autophagic degradation.

Furthermore, our results suggest that the RG group cells are more sensitive than control cells, both in basal conditions and in response to MPP^+ exposure. The data obtained by analyzing different apoptotic parameters agree with the results obtained in a G2019S mutation model (Bravo-San Pedro et al. 2013; Yakhine-Diop et al. 2014). In 2010, Mortiboys et al. reported a reduction in the MMP in fibroblasts from PD patients carrying the G2019S mutation compared to controls of the same age (Mortiboys et al. 2010), as occurs in our model. Likewise, an Arizona group has reported an increase in ROS, a decrease in MMP, and a decrease in cell viability in idiopathic PD fibroblasts (Teves et al. 2017; Yakhine-Diop et al. 2019).

As described in detail in previous studies (Klionsky et al. 2012, 2016), autophagy is a process that requires a delicate functional balance to act as a defense mechanism against multiple stress signals and promote cell survival. Today, a correct autophagy modulation has become the basis of many treatments in the fight against several diseases such as cancer, metabolic and autoimmune disorders, or neurodegenerative disease, including PD (Galluzzi et al. 2017). In the present article, we have attempted to reduce the sensitivity observed in LRRK2 R1441G fibroblasts by modulating autophagic flow, either by blocking it with Baf. A1 or by accelerating it using a nutrient-poor medium (EBSS). We have been able to verify that these treatments not only fail to improve resistance to MPP^+ but also increase the sensitivity of these cells. In summary, fibroblasts from PD patients with the *LRRK2* R1441G mutation present important structural and functional changes in mitochondria and ER, accompanied by high levels of mitochondrial and ER stress that sensitize these cells to neurotoxin treatments. However, RG fibroblasts show basal autophagy, exacerbated lysosomal markers, and interestingly, a dysregulation of autophagy levels that,

added to the mitochondrial and ER stress described above, produces a lethal phenotype upon MPP^+ exposure. The results obtained show the importance that autophagy plays in our model when genetic (R1444G *LRRK2* gene mutation) and environmental factors (exposure to MPP^+) are linked in PD development. However, further in-depth studies are warranted into the mechanisms involved in order to find possible therapeutic targets.

Materials and methods

Cell management

All experiments described were performed between two experimental groups using human fibroblasts as our model: Control (Co, individuals with no PD nor known mutations in the *LRRK2* gene) and R1441G patients (RG, individuals with PD and a R1441G mutation in the *LRRK2* gene). To determine the R1441G LRRK2 mutation in the different group of cell lines, genomic DNA was extracted and digested with the restriction enzyme Bsh1236I (Fig. S1a). Each group contains a pool of three different and non-familial related lines. Before making the pool lines, we determined the expression level of LC3 protein in the control group as well as in the RG group (Fig. S1b, c). After characterization, we selected three control lines and three RG lines based on their similarity to LC3-isoform II expression. We discarded C4 and RG4 as they did not behave in the same way as most of their peers did. Therefore, in this manuscript, we have worked with the cell lines (donor age, sex, genotype) listed in Supplementary Table 1.

All patients gave written consent, and all procedures were approved by the "Comité Ético de Investigación Clínica del Área Sanitaria de Gipuzkoa." Human dermal fibroblasts were isolated as described by Bravo-San Pedro et al. (2013). Cells were maintained in Dulbecco's modified Eagle's medium (DMEM, Gibco, 11,995) supplemented with 10% fetal bovine serum (FBS, Sigma, F7524), 1% 200 mM L-glutamine (Sigma, G7513), and 0.04% V/V penicillin/streptomycin (HyClone, 456–1046). Cells were treated with Baf. A1 (Lclabs, B-1080), BAPTA-AM (Invitrogen, B1212), CCCP (Sigma, C2759), EBSS (Sigma, E2888), MPP^+(Sigma, D048), and rotenone (Sigma, R8875).

Western blot

Human fibroblasts were lysed in a 100 mM Tris–HCl buffer containing NP-40 (0.5% V/V, Roche, 11,754,599,001), 300 mM sodium chloride, and phosphatase and protease inhibitors (Roche, 04,906,837,001 and 1,183,617,001, respectively) (Rodriguez-Arribas et al. 2017a). Proteins were separated on precast 12% Tris–Glycine Mini-PROTEAN TGXTM gels (10 or 15 well, Bio-Rad), and membranes were probed against β-Actin (Abcam, ab49900), autophagy related 5 (ATG5, Cell Signaling, CS2630), Beclin-1 (Santa Cruz, SC-11427), Calnexin (Thermofisher, MA3-027), C/EBP homologous protein (CHOP, Cell Signaling, CS2895), subunit IV of cycloxygenase (COXIV, Abcam, ab14744), cathepsin B (CSTB, Abcam, ab58802), cathepsin D (CSTD, Santa Cruz, SC-6486), dynamin-related protein 1 (DRP1, D6C7, 8570), DJ-1 (MBL, M043-3), phospho-eukaryotic initiation factor 2 subunit alpha (p-eIF2α, Cell Signaling, CS3597), ER oxidoreductins 1 (ERO1, Cell Signaling, CS3274), glyceraldehide-3-phosphate dehydrogenase (GAPDH, Merck-Millipore, MAB374), glucose regulated protein 78 (GRP78/Bip, Cell Signaling, CS3177), iron response element alpha (IREα, Cell Signaling, CS3294), lysosomal-associated membrane protein-1 (LAMP1, Abcam, ab24170), lysosomal-associated membrane protein-2 (LAMP2, Santa Cruz, sc18822), microtubule-associated protein LC3B (LC3-B, Sigma, L7543), lon peptidase 1 (LONP-1, Proteintech, 15,440–1-AP), mitofusin 1 (MFN1, Abcam, ab104274), phospho-mammalian target of rapamycin (p-mTOR, Cell Signaling, CS2971), optineurin (OPTN, Cell Signaling CS58981), sequestosome-1 (p62, Abnova, H0000888-M01), PINK1 (Novus BC100494), prohibitin-1 (PHB1, Cell Signaling CS2426S), p-S6 (Cell Signaling,CS4858), translocase of inner mitochondrial membrane 3 (TIMM23, BD Biosciences, BD611222), translocase of outer mitochondrial membrane 20 (TOMM20, Santa Cruz, SC-17764), or voltage-dependent anion channel-1 (VDAC-1, Abcam, ab14734). HRP-conjugated secondary antibodies targeting mouse (BioRad, 170–6515) or rabbit (BioRad, 170–5047) IgG were used, and images were obtained after luminol oxidation (Pierce, 32,106) with an Amersham i600.

Fluorescence microscopy

Cells were seeded in 24-well plates with coverslips. To assess the involvement of the PINK-1 protein in mitophagy, we transiently transfected our fibroblasts with a PINK1-GFP plasmid using NeuroMag (OZ biosciences, NM50200), according to their protocol. After transfection, cells were incubated, where suitable, with Lysotracker Red® (Invitrogen, L7528) or MitoSOX Red® (Invitrogen, M36008), according to manufacturers' protocols. Cells were immediately fixed with 4% PFA in 1×PBS for 30 min. If primary antibody was needed, cells were permeabilized with 0.1% Triton-X100 (Sigma-Aldrich, T9284) for 10 min, blocked with 1 mg BSA/mL 1×PBS for 30 min, and subsequently incubated with the following primary antibodies for 1 h: Calnexin (Thermofisher, MA3-027), Cyt. *c* (BD Biosciences, BD56432), LAMP2 (Santa Cruz, sc18822), p62 (Abnova, H0000888-M01), or TOMM20 (Santa Cruz, SC-17764). Samples were then treated with their corresponding fluorescence-labeled secondary antibody for 30 min (Invitrogen, A11036 or A11034 for red and green anti-rabbit IgG antibodies; A11004 or A32723 for red and green anti-mouse IgG, respectively). Nuclei were stained with Hoechst 33342 (Sigma, 14533). Images were obtained with an Olympus Ix-51 inverted microscope equipped with a DP-71 camera.

Image analyses

Where suitable, dot measurement was performed with IfDotMeter® software (Rodriguez-Arribas et al. 2016). Intensity measurement was developed in immunofluorescence images using FIJI (Schindelin et al. 2012) "Analyze particles" and "Measure" features with preprogrammed macros to select regions of interest (ROIs) in a semiautomated manner. Colocalization analyses were developed using the JaCoP plugin of ImageJ software with preprogrammed macros. At least 200 ROIs (cells) were analyzed in every experiment.

Flow cytometry

Cells were detached using Trypsin–EDTA (Sigma, T4049), collected into FACS tubes, and loaded with Cyto-ID® (Enzo laboratories, 51,031), $DiOC_{(6)}3$ (Life technologies, D273), Fluo3/AM (Invitrogen, F14218), Mitrotracker green (MTG, Invitrogen, M7514), propidium iodide (PI, Sigma, P4864), or MitoSOX (Invitrogen, M36008) probes to assess different features. Cyto-ID®autophagy detection kit measures autophagic vacuoles and monitors autophagic flux in lysosomally inhibited live cells using a novel dye that selectively labels accumulated autophagic vacuoles. In the case of MTG, this probe concentrates in mitochondria and reacts with the reduced thiols present in mitochondrial matrix proteins independent of altered mitochondrial function or MMP. It has been described that the decrease observed in fluorescence when the probe is preloaded reflects real mitochondrial population levels. So, cells were preloaded with MTG according to a protocol to asses mitophagy (Mauro-Lizcano et al. 2015). Stained cells were analyzed by a flow cytometer (Beckman-Coulter FC500-MPL).

TEM

Following treatment, human fibroblasts were immediately washed with 1×HEPES buffer and fixed with 2% glutaraldehyde in 0.4 M HEPES supplemented with 1% tannic acid. Cells were manually detached, and pellets were subsequently fixed with an osmium tetroxide solution. Samples were desiccated by gradual acetone dilutions and imbibed in an EPON 812 resin. Contrasts were developed with a 2% uranyl acetate solution. Sample cuts were obtained with a Leica EM UC6 ultramicrotome, and images were acquired with a Hitachi S-3600-N microscope.

Quantitative-PCR

mRNA from human fibroblasts was obtained using a RNeasy minikit (Qiagen, 50,974,104) according to the manufacturer's protocol. We synthesized cDNA with the Quantitect Reverse Transcription Kit (Qiagen, 205,311) prior to qPCR using Kappa SYBR Fast Master Mix (Cultek, B4KK4601) in an AB7500 thermocycler. To assess mRNA expression, we used suitable primers from IDT technologies to amplify the genes included in Supplementary Table 2. GAPDH expression was used as a housekeeping gene, and the others were relatively quantified by $2^{(-\Delta\Delta Ct)}$ ratio (Pfaffl 2001).

Statistical analyses

Unless otherwise described, data represent the means ± SD of at least three independent experiments. When

experiments entailed more than two experimental conditions, one-way ANOVA with Bonferroni's post hoc corrections were performed in order to establish differences between cell groups or treatment response. In experiments with two conditions (i.e., control basal vs RG basal), two-tailed Student's T tests were developed with equal or nonequal variances according to Levene's test results. To assess qualitative differences in diffuse Cyt. *c* and nuclei condensation, Chi-square's tests were employed between control and R1441G groups for each condition considered. Significance in these tests are expressed as * ($p<0.05$), ** ($p<0.01$) *** ($p<0.001$) when comparing groups or # ($p<0.05$), ## ($p<0.01$), ($p<0.001$) when comparing treatments.

Abbreviations *Baf. A1*, Bafilomycin A1 (Baf. A1); *CCCP,* Carbonyl cyanide 3-chlorophenylhydrazone; *EBSS,* Earle's balanced salt solution; *ER*, Endoplasmic reticulum; *LRRK2*, Leucine-rich repeat kinase 2; *LTR*, Lysotracker red; *MAMs*, Mitochondria-associated ER membranes; *MPP^+,* 1-Methyl-4-phenylpiridinium; PD, Parkinson's disease; PINK1, PTEN-induced putative kinase 1; ROS, Reactive oxygen species; TOMM20, Translocase of outer mitochondrial membrane 20;

Acknowledgements The authors thank M.P. Delgado-Luceño and FUNDESALUD for helpful assistance and are grateful to the patients and donors for their participation.

Author contribution RAGP, JMF, and MNS designed the study and wrote the publication with help of JMBSP, MRA, and SMSYD. SMSYD, MRA, and SCC carried out most the lab experiments. GMC, EUC, MBB, GDG, MPB, and EAC provided help with the experiments. VC provided technical assistance with electron microscopy studies. AA and ALM provided the fibroblast model from patient biopsies. All authors have read and approved the final manuscript.

Funding This research was supported by the "Instituto de Salud Carlos" III CIBERNED (CB06/05/0041 and PI14/00170) and partially supported by the "Fondo Europeo de Desarrollo Regional" (FEDER) from the European Union. S.M.S.Y-D was supported by CIBERNED. S. C-C and E.U-C are supported by a FPU fellowship (FPU19/04435 and FPU16/00684, respectively) from the Ministerio de Ciencia, Innovación y Universidades, Spain. G. M-C is supported by University of Extremadura (ONCE Foundation). M. B-B is supported by a collaboration grant from the Ministerio de Educación y Formación Profesional, Spain. G. D-G is supported by the Consejería de Educación y Empleo-SEXPE-Fondo Social Europeo (TE-0031-19). M. P-B is a recipient of a fellowship from the "Plan Propio de Iniciación a la Investigación, Desarrollo Tecnológico e Innovación (University of Extremadura)". E.A-C is supported by a grant (IB18048) from the Junta de Extremadura, Spain. M.N-S and J.M-B. S-P were funded by the "Ramon y Cajal" Program (RYC-2016–20883 and RYC-2018–025099, respectively), Spain.

Supplementary Information The online version contains supplementary material available at https://doi.org/10.1007/s10565-021-09617-w.

Availability of data and material The datasets used and/or analyzed during the current study are available from the corresponding author on reasonable request.

Code availability Not applicable.

Declarations

Ethics approval All patients gave written consent, and all procedures were approved by the "Comité Ético de Investigación Clínica del Área Sanitaria de Gipuzkoa," Spain.

Consent to participate Not applicable.

Consent for publication Not applicable.

Conflict of interest The authors declare no competing interests.

References

Bezprozvanny I. Calcium signaling and neurodegenerative diseases. Trends Mol Med. 2009;15:89–100.

Bonello F, Hassoun SM, Mouton-Liger F, Shin YS, Muscat A, Tesson C, Lesage S, Beart PM, Brice A, Krupp J, et al. LRRK2 impairs PINK1/Parkin-dependent mitophagy via its kinase activity: pathologic insights into Parkinson's disease. Hum Mol Genet. 2019;28:1645–60.

Bravo-San Pedro JM, Niso-Santano M, Gomez-Sanchez R, Pizarro-Estrella E, Aiastui-Pujana A, Gorostidi A, Climent V, Lopez de Maturana R, Sanchez-Pernaute R, Lopez de Munain A, et al. The LRRK2 G2019S mutant exacerbates basal autophagy through activation of the MEK/ERK pathway. Cell Mol Life Sci. 2013;70:121–36.

Burte F, Carelli V, Chinnery PF, Yu-Wai-Man P. Disturbed mitochondrial dynamics and neurodegenerative disorders. Nat Rev Neurol. 2015;11:11–24.

Cali T, Ottolini D, Negro A, Brini M. Enhanced parkin levels favor ER-mitochondria crosstalk and guarantee Ca(2+) transfer to sustain cell bioenergetics. Biochim Biophys Acta. 2013;1832:495–508.

Canet-Aviles RM, Wilson MA, Miller DW, Ahmad R, McLendon C, Bandyopadhyay S, Baptista MJ, Ringe D, Petsko GA, Cookson MR. The Parkinson's disease protein DJ-1 is neuroprotective due to cysteine-sulfinic acid-driven mitochondrial localization. Proc Natl Acad Sci U S A. 2004;101:9103–8.

Cerri S, Blandini F. Role of autophagy in Parkinson's disease. Curr Med Chem. 2019;26:3702–18.

Cherra SJ 3rd, Steer E, Gusdon AM, Kiselyov K, Chu CT. Mutant LRRK2 elicits calcium imbalance and depletion of dendritic mitochondria in neurons. Am J Pathol. 2013;182:474–84.

Cho HJ, Yu J, Xie C, Rudrabhatla P, Chen X, Wu J, Parisiadou L, Liu G, Sun L, Ma B, et al. Leucine-rich repeat kinase 2 regulates Sec16A at ER exit sites to allow ER-Golgi export. EMBO J. 2014;33:2314–31.

Chung SY, Kishinevsky S, Mazzulli JR, Graziotto J, Mrejeru A, Mosharov EV, Puspita L, Valiulahi P, Sulzer D, Milner TA, et al. Parkin and PINK1 patient iPSC-derived midbrain dopamine neurons exhibit mitochondrial dysfunction and alpha-synuclein accumulation. Stem Cell Reports. 2016;7:664–77.

Cuervo AM, Stefanis L, Fredenburg R, Lansbury PT, Sulzer D. Impaired degradation of mutant alpha-synuclein by chaperone-mediated autophagy. Science. 2004;305:1292–5.

de Brito OM, Scorrano L. Mitofusin 2 tethers endoplasmic reticulum to mitochondria. Nature. 2008;456:605–10.

Fonseca TB, Sanchez-Guerrero A, Milosevic I, Raimundo N. Mitochondrial fission requires DRP1 but not dynamins. Nature. 2019;570:E34–42.

Galluzzi L, Bravo-San Pedro JM, Levine B, Green DR, Kroemer G. Pharmacological modulation of autophagy: therapeutic potential and persisting obstacles. Nat Rev Drug Discov. 2017;16:487–511.

Ganguly U, Chakrabarti SS, Kaur U, Mukherjee A, Chakrabarti S. Alpha-synuclein, proteotoxicity and Parkinson's disease: search for neuroprotective therapy. Curr Neuropharmacol. 2018;16:1086–97.

Giacomello M, Pyakurel A, Glytsou C, Scorrano L. The cell biology of mitochondrial membrane dynamics. Nat Rev Mol Cell Biol. 2020;21:204–24.

Gomez-Suaga P, Luzon-Toro B, Churamani D, Zhang L, Bloor-Young D, Patel S, Woodman PG, Churchill GC, Hilfiker S. Leucine-rich repeat kinase 2 regulates autophagy through a calcium-dependent pathway involving NAADP. Hum Mol Genet. 2012;21:511–25.

Gomez-Suaga P, Rivero-Rios P, Fdez E, Blanca Ramirez M, Ferrer I, Aiastui A, Lopez De Munain A, Hilfiker S. LRRK2 delays degradative receptor trafficking by impeding late endosomal budding through decreasing Rab7 activity. Hum Mol Genet. 2014;23:6779–96.

Gomez-Suaga P, Bravo-San Pedro JM, Gonzalez-Polo RA, Fuentes JM, Niso-Santano M. ER-mitochondria signaling in Parkinson's disease. Cell Death Dis. 2018;9:337.

Greggio E, Taymans JM, Zhen EY, Ryder J, Vancraenenbroeck R, Beilina A, Sun P, Deng J, Jaffe H, Baekelandt V, et al. The Parkinson's disease kinase LRRK2 autophosphorylates its GTPase domain at multiple sites. Biochem Biophys Res Commun. 2009;389:449–54.

Hsieh CH, Shaltouki A, Gonzalez AE, Bettencourt da Cruz A, Burbulla LF, St Lawrence E, Schule B, Krainc D, Palmer TD, Wang X. Functional impairment in miro degradation and mitophagy is a shared feature in familial and sporadic Parkinson's disease. Cell Stem Cell. 2016;19:709–24.

Ivankovic D, Chau KY, Schapira AH, Gegg ME. Mitochondrial and lysosomal biogenesis are activated following PINK1/parkin-mediated mitophagy. J Neurochem. 2016;136:388–402.

Kania E, Pajak B, Orzechowski A. Calcium homeostasis and ER stress in control of autophagy in cancer cells. Biomed Res Int. 2015;2015:352794.

Kitzman HH Jr, McMahon RJ, Aslanian AM, Fadia PM, Frost SC. Differential regulation of GRP78 and GLUT1 expression in 3T3-L1 adipocytes. Mol Cell Biochem. 1996;162:51–8.

Klionsky DJ, Abdalla FC, Abeliovich H, Abraham RT, Acevedo-Arozena A, Adeli K, Agholme L, Agnello M, Agostinis P, Aguirre-Ghiso JA, et al. Guidelines for the use and interpretation of assays for monitoring autophagy. Autophagy. 2012;8:445–544.

Klionsky DJ, Abdelmohsen K, Abe A, Abedin MJ, Abeliovich H, Acevedo Arozena A, Adachi H, Adams CM, Adams PD, Adeli K, et al. Guidelines for the use and interpretation of assays for monitoring autophagy (3rd edition). Autophagy. 2016;12:1–222.

Koentjoro B, Park JS, Sue CM. Nix restores mitophagy and mitochondrial function to protect against PINK1/Parkin-related Parkinson's disease. Sci Rep. 2017;7:44373.

Larsen SB, Hanss Z, Kruger R. The genetic architecture of mitochondrial dysfunction in Parkinson's disease. Cell Tissue Res. 2018;373:21–37.

Lavalley NJ, Slone SR, Ding H, West AB, Yacoubian TA. 14-3-3 Proteins regulate mutant LRRK2 kinase activity and neurite shortening. Hum Mol Genet. 2016;25:109–22.

Lee KS, Huh S, Lee S, Wu Z, Kim AK, Kang HY, Lu B. Altered ER-mitochondria contact impacts mitochondria calcium homeostasis and contributes to neurodegeneration in vivo in disease models. Proc Natl Acad Sci U S A. 2018;115:E8844–53.

Lee JH, Han JH, Kim H, Park SM, Joe EH, Jou I. Parkinson's disease-associated LRRK2-G2019S mutant acts through regulation of SERCA activity to control ER stress in astrocytes. Acta Neuropathol Commun. 2019;7:68.

Lievremont JP, Rizzuto R, Hendershot L, Meldolesi J. BiP, a major chaperone protein of the endoplasmic reticulum lumen, plays a direct and important role in the storage of the rapidly exchanging pool of Ca2+. J Biol Chem. 1997;272:30873–9.

Lin D, Liang Y, Zheng D, Chen Y, Jing X, Lei M, Zeng Z, Zhou T, Wu X, Peng S, et al. Novel biomolecular information in rotenone-induced cellular model of Parkinson's disease. Gene. 2018;647:244–60.

Liu HF, Lu S, Ho PW, Tse HM, Pang SY, Kung MH, Ho JW, Ramsden DB, Zhou ZJ, Ho SL. LRRK2 R1441G mice are more liable to dopamine depletion and locomotor inactivity. Annals of Clinical and Translational Neurology. 2014;1:199–208.

Lopez de Maturana R, Lang V, Zubiarrain A, Sousa A, Vazquez N, Gorostidi A, Aguila J, Lopez de Munain A, Rodriguez M, Sanchez-Pernaute R. Mutations in LRRK2 impair NF-kappaB pathway in iPSC-derived neurons. J Neuroinflammation. 2016;13:295.

Lynch-Day MA, Mao K, Wang K, Zhao M, Klionsky DJ. The role of autophagy in Parkinson's disease. Cold Spring Harb Perspect Med. 2012;2:a009357.

Manzoni C. The LRRK2-macroautophagy axis and its relevance to Parkinson's disease. Biochem Soc Trans. 2017;45:155–62.

Manzoni C, Mamais A, Dihanich S, Abeti R, Soutar MPM, Plun-Favreau H, Giunti P, Tooze SA, Bandopadhyay R, Lewis PA. Inhibition of LRRK2 kinase activity stimulates macroautophagy. Biochim Biophys Acta. 2013a;1833:2900–10.

Manzoni C, Mamais A, Dihanich S, McGoldrick P, Devine MJ, Zerle J, Kara E, Taanman JW, Healy DG, Marti-Masso JF, et al. Pathogenic Parkinson's disease mutations across the functional domains of LRRK2 alter the autophagic/lysosomal response to starvation. Biochem Biophys Res Commun. 2013b;441:862–6.

Martin I, Kim JW, Dawson VL, Dawson TM. LRRK2 pathobiology in Parkinson's disease. J Neurochem. 2014;131:554–65.

Martinez JH, Alaimo A, Gorojod RM, Porte Alcon S, Fuentes F, Coluccio Leskow F, Kotler ML. Drp-1 dependent mitochondrial fragmentation and protective autophagy in dopaminergic SH-SY5Y cells overexpressing alpha-synuclein. Mol Cell Neurosci. 2018;88:107–17.

Mattson MP. Calcium and neurodegeneration. Aging Cell. 2007;6:337–50.

Mauro-Lizcano M, Esteban-Martinez L, Seco E, Serrano-Puebla A, Garcia-Ledo L, Figueiredo-Pereira C, Vieira HL, Boya P. New method to assess mitophagy flux by flow cytometry. Autophagy. 2015;11:833–43.

McCoy MK, Cookson MR. DJ-1 regulation of mitochondrial function and autophagy through oxidative stress. Autophagy. 2011;7:531–2.

Melser S, Lavie J, Benard G. Mitochondrial degradation and energy metabolism. Biochim Biophys Acta. 2015;1853:2812–21.

Mercado G, Castillo V, Soto P, Lopez N, Axten JM, Sardi SP, Hoozemans JJM, Hetz C. Targeting PERK signaling with the small molecule GSK2606414 prevents neurodegeneration in a model of Parkinson's disease. Neurobiol Dis. 2018;112:136–48.

Michel PP, Hirsch EC, Hunot S. Understanding dopaminergic cell death pathways in Parkinson disease. Neuron. 2016;90:675–91.

Mishra P, Chan DC. Metabolic regulation of mitochondrial dynamics. J Cell Biol. 2016;212:379–87.

Mortiboys H, Johansen KK, Aasly JO, Bandmann O. Mitochondrial impairment in patients with Parkinson disease with the G2019S mutation in LRRK2. Neurology. 2010;75:2017–20.

Niu J, Yu M, Wang C, Xu Z. Leucine-rich repeat kinase 2 disturbs mitochondrial dynamics via Dynamin-like protein. J Neurochem. 2012;122:650–8.

Orenstein SJ, Kuo SH, Tasset I, Arias E, Koga H, Fernandez-Carasa I, Cortes E, Honig LS, Dauer W, Consiglio A, et al. Interplay of LRRK2 with chaperone-mediated autophagy. Nat Neurosci. 2013;16:394–406.

Papkovskaia TD, Chau KY, Inesta-Vaquera F, Papkovsky DB, Healy DG, Nishio K, Staddon J, Duchen MR, Hardy J, Schapira AH, Cooper JM. G2019S leucine-rich repeat kinase 2 causes uncoupling protein-mediated mitochondrial depolarization. Hum Mol Genet. 2012;21:4201–13.

Pfaffl MW. A new mathematical model for relative quantification in real-time RT-PCR. Nucleic Acids Res. 2001;29:e45.

Plowey ED, Cherra SJ 3rd, Liu YJ, Chu CT. Role of autophagy in G2019S-LRRK2-associated neurite shortening in differentiated SH-SY5Y cells. J Neurochem. 2008;105:1048–56.

Rodriguez-Arribas M, Pizarro-Estrella E, Gomez-Sanchez R, Yakhine-Diop SM, Gragera-Hidalgo A, Cristo A, Bravo-San Pedro JM, Gonzalez-Polo RA, Fuentes JM. IFDOTMETER: a new software application for automated immunofluorescence analysis. J Lab Autom. 2016;21:246–59.

Rodriguez-Arribas M, Yakhine-Diop SM, Gonzalez-Polo RA, Niso-Santano M, Fuentes JM. Turnover of lipidated LC3 and autophagic cargoes in mammalian cells. Methods Enzymol. 2017a;587:55–70.

Rodriguez-Arribas M, Yakhine-Diop SMS, Pedro JMB, Gomez-Suaga P, Gomez-Sanchez R, Martinez-Chacon G, Fuentes JM, Gonzalez-Polo RA, Niso-Santano M. Mitochondria-associated membranes (MAMs): overview and its role in Parkinson's disease. Mol Neurobiol. 2017b;54:6287–303.

Saez-Atienzar S, Bonet-Ponce L, Blesa JR, Romero FJ, Murphy MP, Jordan J, Galindo MF. The LRRK2 inhibitor GSK2578215A induces protective autophagy in SH-SY5Y cells: involvement of Drp-1-mediated mitochondrial fission and mitochondrial-derived ROS signaling. Cell Death Dis. 2014;5:e1368.

Sahani MH, Itakura E, Mizushima N. Expression of the autophagy substrate SQSTM1/p62 is restored during prolonged starvation depending on transcriptional upregulation and autophagy-derived amino acids. Autophagy. 2014;10:431–41.

Samann J, Hegermann J, von Gromoff E, Eimer S, Baumeister R, Schmidt E. Caenorhabditits elegans LRK-1 and PINK-1 act antagonistically in stress response and neurite outgrowth. J Biol Chem. 2009;284:16482–91.

Schapira AH. Mitochondria in the aetiology and pathogenesis of Parkinson's disease. Lancet Neurol. 2008;7:97–109.

Schindelin J, Arganda-Carreras I, Frise E, Kaynig V, Longair M, Pietzsch T, Preibisch S, Rueden C, Saalfeld S, Schmid B, et al. Fiji: an open-source platform for biological-image analysis. Nat Methods. 2012;9:676–82.

Schwab AJ, Sison SL, Meade MR, Broniowska KA, Corbett JA, Ebert AD. Decreased sirtuin deacetylase activity in LRRK2 G2019S iPSC-derived dopaminergic neurons. Stem Cell Reports. 2017;9:1839–52.

Somme JH, Molano Salazar A, Gonzalez A, Tijero B, Berganzo K, Lezcano E, Fernandez Martinez M, Zarranz JJ, Gomez-Esteban JC. Cognitive and behavioral symptoms in Parkinson's disease patients with the G2019S and R1441G mutations of the LRRK2 gene. Parkinsonism Relat Disord. 2015;21:494–9.

Su YC, Qi X. Inhibition of excessive mitochondrial fission reduced aberrant autophagy and neuronal damage caused by LRRK2 G2019S mutation. Hum Mol Genet. 2013;22:4545–61.

Su YC, Guo X, Qi X. Threonine 56 phosphorylation of Bcl-2 is required for LRRK2 G2019S-induced mitochondrial depolarization and autophagy. Biochim Biophys Acta. 2015;1852:12–21.

Tagliaferro P, Kareva T, Oo TF, Yarygina O, Kholodilov N, Burke RE. An early axonopathy in a hLRRK2(R1441G) transgenic model of Parkinson disease. Neurobiol Dis. 2015;82:359–71.

Teves JMY, Bhargava V, Kirwan KR, Corenblum MJ, Justiniano R, Wondrak GT, Anandhan A, Flores AJ, Schipper DA, Khalpey Z, et al. Parkinson's disease skin fibroblasts display signature alterations in growth, redox homeostasis, mitochondrial function, and autophagy. Front Neurosci. 2017;11:737.

Toyofuku T, Okamoto Y, Ishikawa T, Sasawatari S, Kumanogoh A. LRRK2 regulates endoplasmic reticulum-mitochondrial tethering through the PERK-mediated ubiquitination pathway. EMBO J. 2020;39:e100875.

van der Merwe C, Jalali Sefid Dashti Z, Christoffels A, Loos B, Bardien S. Evidence for a common biological pathway linking three Parkinson's disease-causing genes: parkin, PINK1 and DJ-1. Eur J Neurosci. 2015;41:1113–25.

Wang X, Yan MH, Fujioka H, Liu J, Wilson-Delfosse A, Chen SG, Perry G, Casadesus G, Zhu X. LRRK2 regulates mitochondrial dynamics and function through direct interaction with DLP1. Hum Mol Genet. 2012;21:1931–44.

Weil R, Laplantine E, Curic S, Genin P. Role of optineurin in the mitochondrial dysfunction: potential implications in neurodegenerative diseases and cancer. Front Immunol. 2018;9:1243.

Williams JA, Hou Y, Ni HM, Ding WX. Role of intracellular calcium in proteasome inhibitor-induced endoplasmic reticulum stress, autophagy, and cell death. Pharm Res. 2013;30:2279–89.

Wong DP, Chu JM, Hung VK, Lee DK, Cheng CH, Yung KK, Yue KK. Modulation of endoplasmic reticulum chaperone GRP78 by high glucose in hippocampus of streptozotocin-induced diabetic mice and C6 astrocytic cells. Neurochem Int. 2013;63:551–60.

Yakhine-Diop SM, Bravo-San Pedro JM, Gomez-Sanchez R, Pizarro-Estrella E, Rodriguez-Arribas M, Climent V, Aiastui A, Lopez de Munain A, Fuentes JM, Gonzalez-Polo RA. G2019S LRRK2 mutant fibroblasts from Parkinson's disease patients show increased sensitivity to neurotoxin 1-methyl-4-phenylpyridinium dependent of autophagy. Toxicology. 2014;324:1–9.

Yakhine-Diop SMS, Niso-Santano M, Rodriguez-Arribas M, Gomez-Sanchez R, Martinez-Chacon G, Uribe-Carretero E, Navarro-Garcia JA, Ruiz-Hurtado G, Aiastui A, Cooper JM, et al. Impaired mitophagy and protein acetylation levels in fibroblasts from Parkinson's disease patients. Mol Neurobiol. 2019;56:2466–81.

Yang S, Xia C, Li S, Du L, Zhang L, Hu Y. Mitochondrial dysfunction driven by the LRRK2-mediated pathway is associated with loss of Purkinje cells and motor coordination deficits in diabetic rat model. Cell Death Dis. 2014;5:e1217.

Yuan Y, Cao P, Smith MA, Kramp K, Huang Y, Hisamoto N, Matsumoto K, Hatzoglou M, Jin H, and Feng Z. Dysregulated LRRK2 signaling in response to endoplasmic reticulum stress leads to dopaminergic neuron degeneration in C. elegans. PLoS One. 2011;6:e22354.

Zhu Y, Wang C, Yu M, Cui J, Liu L, Xu Z. ULK1 and JNK are involved in mitophagy incurred by LRRK2 G2019S expression. Protein Cell. 2013;4:711–21.

Zurita Rendon O, and Shoubridge EA. LONP1 is required for maturation of a subset of mitochondrial proteins, and its loss elicits an integrated stress response. Mol Cell Biol. 2018;38.